Pose and Position Trajectory Tracking for Aerial Transportation of a Rod-Like Object

Pedro Pereira[a], Dimos V. Dimarogonas[a]

[a]*School of Electrical Engineering, KTH Royal Institute of Technology, Stockholm, Sweden.*

Abstract

This paper focuses on a pose tracking problem for a system composed of two connected rigid bodies, namely an aerial vehicle – with hovering capabilities – and a rod-like rigid body. The rod-like rigid body has an axis of axial symmetry, and the joint connecting the aerial vehicle and the rod lies along that axis. The aerial vehicle is meant to transport that object, which can swing/slung with respect to the vehicle: we refer to this as generalized slung load transportation because the object being transported is a rod-like object, as opposed to standard slung load transportation where the object is a point mass with no moment of inertia. Given this system, we consider two tracking problems. Firstly, we assume that a torque input on the joint is available, and, for this scenario, we formulate a *semi*-pose tracking problem, requiring the rod object to track a desired pose trajectory, apart from rotations around its axis of axial symmetry (and thus the *semi* qualifier). Secondly, we assume that no such torque input is available, and, for this scenario, we formulate a position tracking problem, requiring a specific point along the axis of axial symmetry of the rod object to track a desired position trajectory. Our approach for solving both these problems lies in finding a state and an input transformations, such that the vector field in the new coordinates is of a known form for which controllers are found in the literature, and which we leverage in this paper. Simulations are presented that validate the proposed algorithms.

1. Introduction

Unmanned aerial vehicles (UAVs) provide a platform for performing and testing a variety of tasks: UAVs have been used to map large surface areas, to surveil dangerous terrains, and to inspect remote infrastructures [1–3]. More recently, UAVs with hovering capabilities have been successfully employed in transporting cargoes, which is of interest in dangerous and cluttered environments [4, 5].

Aerial transportation may be categorized as slung-load or tethered transportation [5–19] *vs* manipulator-endowed transportation [3, 20–27]; and as single-UAV transportation *vs* multiple-UAV transportation. Slung-load/tethered transportation, when compared with transportation by manipulators, is mechanically simple, inexpensive, and it does not require any power supply; manipulator-endowed transportation, on the other hand, provides extra degrees of freedom which can be used to perform more complex tasks – such as picking up an object from inside a drawer [21]. In cluttered environments, transportation with a single UAV may be the only feasible option, while transportation with multiple UAVs is primarily necessary when the cargo exceeds the individual UAVs' payload capacity. Aerial transportation is particularly important in scenarios where human intervention should be minimized: collection of samples in dangerous environments, delivery of supplies in flooded areas, and inspection of aging infrastructures are among potential applications. In this paper, the system at study is composed of a single UAV connected to a rod-like object, and two different cases are considered: in the first case, we assume a torque input at the joint connecting the UAV and the object is available, thus falling into the manipulator-endowed transportation – see Fig. 1a; in the second case, no such torque is made available, thus falling into the slung-load/tethered transportation – see Fig. 1b.

Different aspects of aerial transportation have been considered in the literature. In slung-load transportation, vision and force sensors have been used to estimate the swing angle of the load, or to autonomously estimate the cargo's pose, which is then used in the feedback loop to avoid/dampen swing excitation [6–8, 28]; in manipulator-endowed transportation, vision has been used to correctly place end-effectors with respect to a visual target placed on the object to be transported [8, 29, 30]. Differential flatness has been used for the purposes of motion control [11, 24, 31–34], such as planning trajectories that minimize the loads' swing. Motion planning for collision avoidance between the cargo and the UAVs with obstacles has also been studied and validated [14, 22, 23, 35]. Adaptive and robust controllers have also been proposed, which estimate and compensate for the static and dynamic effects of the cargo on the UAV [5, 25–27]. In multiple-UAV transportation, controllers exploiting a master-slave paradigm have also been considered [36].

In aerial tethered transportation, a cable establishes a

[☆]The authors are with the School of Electrical Engineering, KTH Royal Institute of Technology, SE-100 44, Stockholm, Sweden. Email addresses: {ppereira, dimos}@kth.se. This work was supported by the EU H2020 Research and Innovation Programme under GA No.644128 (AEROWORKS), the Swedish Research Council (VR), the Swedish Foundation for Strategic Research (SSF) and the KAW Foundation.

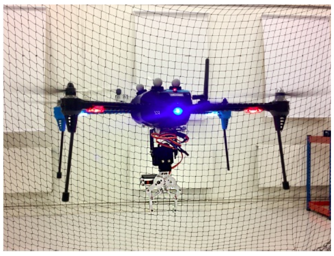

(a) Manipulator that can be modeled as a rod-like rigid body, and with a torque input available at the joint connecting the manipulator to the aerial vehicle.

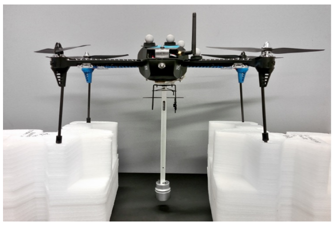

(b) A rod-like object connected to an aerial vehicle at a point along the axis of axial symmetry: the rod object may be interpreted as an un-actuated manipulator.

Figure 1: Real system composed of an aerial vehicle (Iris+ from 3D Robotics) and a manipulator/rod-like-object [38].

physical connection between the UAV and the load, and, under tensile forces, it behaves like an un-actuated manipulator (i.e., like a rigid link). To be specific, under tensile forces, the cable imposes a holonomic restriction, namely that the distance between the UAV and the load is equal to the cable length; if that is not the case, no such restriction applies, and the UAV and the load can move independently. In the literature of tethered transportation, some works have focused on the hybrid modeling describing the dynamics when the cable is taut and when it is not, and hybrid controllers have also been proposed that deal with the hybrid dynamics [10, 11, 37]. In this paper, we model the rod-like object as a rigid three-dimensional pendulum that, rather than attached to a fixed pivot-point, is attached to a moving one, namely the UAV – see Fig. 1b. Because the rod is rigid, it can withstand compression forces, and the need for a hybrid model is unnecessary. Nonetheless, this paper's results apply for tethered transportation, provided that the cable remains under tensile forces[1].

1.1. Paper's organization

In Section 3, we model our system composed of two rigid bodies, namely a UAV and a rod-like object. We consider two systems, one where there is a torque input at the joint connecting the rigid bodies – UAV-manipulator system (Fig. 1a); and one where there is not – UAV-slung-manipulator system (Fig. 1b). In Subection 3.1, we formulate the problem statement for the UAV-manipulator system, and in Subection 3.2, we formulate the problem statement for the UAV-slung-manipulator system. In Section 4, we explain the control strategy for both problems; and in Section 5, we implement that strategy for the UAV-manipulator system, while in Section 6 we implement that same strategy for the UAV-slung-manipulator system. Finally, in Section 7, we provide some illustrative simulations. In [39], one finds mathematica files that corroborate all of the presented results.

1.2. Contributions

Let us summarize some of this paper's contributions. First of all, we note that the considered system is not fully actuated, and thus inverse dynamics control – where a nonlinear control law linearizes and decouples the system [40] – cannot be implemented.

One of our contributions lies in analyzing two problems under a common framework: namely, we consider a UAV-manipulator system and a UAV-slung-manipulator system, which are the same system, with the exception that the UAV-slung-manipulator system is deprived of a torque input (and thus the *slung* in the naming). The UAV-manipulator system is mechanically more complex than the UAV-slung-manipulator system, as it requires a source for torque actuation at the ball joint: as such, the UAV-manipulator system is of use in circumstances where the collection of the load requires a precise positioning of the manipulator, while the UAV-slung-manipulator system is a better option when the load is easy to collect (with the help of an electromagnet, for example).

Another main contribution, with respect to the UAV-manipulator system, lies in showing that it is equivalent to two decoupled subsystems: one concerning the position of the center-of-mass of the system, and another concerning the attitude of the manipulator. The first subsystem has the dynamics of a VTOL vehicle, and thus we are able to leverage controllers from the literature to control the position of the center-of-mass [41–45]. The second subsystem has the dynamics of a second order system in the unit sphere, and thus we are able to leverage controllers from the literature to control the attitude of the manipulator [46–48].

Equivalently, another main contribution, this time with respect to the UAV-slung-manipulator system, lies in showing that it is equivalent to a VTOL vehicle cascaded after a second order system in the unit sphere. For this system, we are also able to leverage controllers for VTOL vehicles from the literature, which must be complemented with two backstepping steps (related to the second order system). We emphasize that this system is a generalization of the slung load system: indeed, rather than a point mass, the aerial vehicle carries a rigid body with some moment of inertia, with the slung load problem being recovered if that

[1] In order to guarantee that the cable remains under tensile forces, one needs to impose proper constraints on the desired trajectory, on the chosen control laws, and on the set of initial conditions. Suppose, e.g., that the UAV is above the load: if, initially, the load moves with a large upward velocity and the UAV moves with a large downward velocity, then the cable would need to be under compression so as to prevent the UAV and load from approaching each other; while a manipulator can provide such a compressive force, a cable cannot.

moment of inertia vanishes.

This work provides an extension of the results found in [38] and [49], the first related to manipulator-endowed transportation and the latter to slung transportation. This paper unifies those two problems, while generalizing them at the same time. To be specific, in [38] and [49], the load is taken to be a point-mass, whilst in this paper it is taken as a rod-like object with non-zero inertia. For both problems, the yaw motion of the UAV and of the manipulator may be treated as separate problems, and thus we introduce an equivalence relation which *does not see* those motions, and we perform the analysis in the quotient space. This also constitutes another contribution of this paper.

2. Notation

The map $\mathcal{S} : \mathbb{R}^3 \to \mathbb{R}^{3\times3}$ yields a skew-symmetric matrix and it satisfies $\mathcal{S}(a)\, b := a \times b$, for any $a, b \in \mathbb{R}^3$. $\mathbb{S}^n := \{x \in \mathbb{R}^{n+1} : x^T x = 1\}$ denotes the set of unit vectors in $\mathbb{R}^{n+1}$. The map $\Pi : \mathbb{S}^2 \ni x \mapsto \Pi(x) := I_3 - xx^T \in \mathbb{R}^{3\times3}$ yields a matrix that represents the projection onto the subspace orthogonal to $x \in \mathbb{S}^2$. Denote $d_{\mathbb{R}^n} : \mathbb{R}^n \times \mathbb{R}^n \ni (a, b) \mapsto d_{\mathbb{R}^n}(a, b) := \|a-b\| \in \mathbb{R}_{\geq 0}$ as the standard distance in $\mathbb{R}^n$. Denote $A_1 \oplus \cdots \oplus A_n$ as the block diagonal matrix with block diagonal entries A_1 to A_n (square matrices). We denote by $e_1, \cdots, e_n \in \mathbb{R}^n$ the canonical basis vectors in $\mathbb{R}^n$; when clear from the context the Eucledian space the vectors belong to is omitted. For some set A, $\mathrm{id}_A : A \ni x \mapsto \mathrm{id}_A(x) := x \in A$ denotes the identity map on that set. Given some normed spaces A and B, and a function $f : A \ni a \mapsto f(a) \in B$, $Df : A \ni a \mapsto Df(a) \in \mathcal{L}(A, B)$ denotes the derivative of f ($\mathcal{L}(A, B)$ denotes the set of linear maps from A to B). Given a manifold A, $T_a A$ denotes the tangent set of A at a point $a \in A$. Finally, throughout the paper, we use symbols in pairs (e.g., Ω and ω), with the upper-case symbol being associated to the aerial vehicle, and the lower-case symbol being associated to the manipulator.

3. Modeling and Problem Statement

Consider the system illustrated in Fig. 2, composed of two rigid bodies, namely one aerial vehicle (which, for brevity, we refer to as UAV hereafter) and a manipulator (with a load at its end-effector). The two rigid bodies are coupled, with a ball-joint connecting them at the center-of-mass of the UAV. If the ball-joint were absent, the manipulator would behave as a free falling (un-actuated) rigid body, and the UAV would behave as a *standard* UAV. In its presence, the ball-joint imposes a kinematic constraint, specifically, it enforces the UAV's position to be fixed in the manipulator's orientation frame. This kinematic constraint *links* the UAV and the manipulator, and it provides a way to control the manipulator by means of actuation on the UAV.

For brevity, let us list the physical constants that describe the system (we use upper-case symbols for the UAV's constants, and lower-case symbols for the manipulator's): $l > 0$ is the distance between the rigid bodies centers-of-mass; $M > 0$ and $J \in \mathbb{R}^{3\times3}$ are the UAV's mass and moment of inertia; $m > 0$ and

$$j := j_{xy} \oplus j_{xy} \oplus j_{zz} \in \mathbb{R}^{3\times3} \tag{1}$$

are the manipulator's mass and moment of inertia. Denote the pose and twist of the system as the pair of poses and twists of the individual rigid bodies, i.e.,

$$\mathcal{P} \in \mathbb{SE}(3)^{\times2} :\Leftrightarrow ((p, r), (P, R)) \in \mathbb{SE}(3)\times\mathbb{SE}(3), \tag{2a}$$

$$\mathcal{V} \in \mathbb{R}^{12} :\Leftrightarrow ((v, \omega), (V, \Omega)) \in (\mathbb{R}^3)^2 \times (\mathbb{R}^3)^2. \tag{2b}$$

where $(P, R)/(p, r) \in \mathbb{R}^3\times\mathbb{SO}(3)$ is the UAV/manipulator's pose (linear and angular positions); and $(V, \Omega)/(v, \omega) \in \mathbb{R}^3\times\mathbb{R}^3$ is the UAV/manipulator's twist (linear and angular velocities). Finally, let us list the inputs that act on the system, and for which we propose control laws later: $U \in \mathbb{R}$ is the UAV's thrust input; $\tau \in \mathbb{R}^3$ is the body frame UAV's torque input; $\tau_m \in \mathbb{R}^3$ is the body frame manipulator's torque input.

We let the state be composed of the system's pose and twist as defined in (2a) and (2b), and define the state space as

$$\mathbb{X} := \big\{(\mathcal{P}, \mathcal{V}) \in \mathbb{SE}(3)^{\times2} \times \mathbb{R}^{12} : \tag{3}$$
$$p + lre_3 - P = 0_3, v + lr\mathcal{S}(\omega)\, e_3 - V = 0_3\big\},$$

which encapsulates the constraints imposed by the ball-joint, specifically, that the UAV's position is fixed w.r.t. the manipulator's orientation frame, i.e., that $r^T(P - p) = le_3 \Leftrightarrow p + lre_3 - P = 0_3$ (recall that $r \in \mathbb{SO}(3)$ represents the manipulator's orientation frame). Hereafter, we always

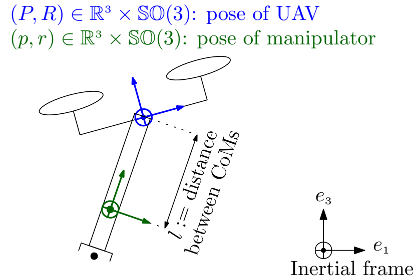

(a) Poses of UAV and manipulator.

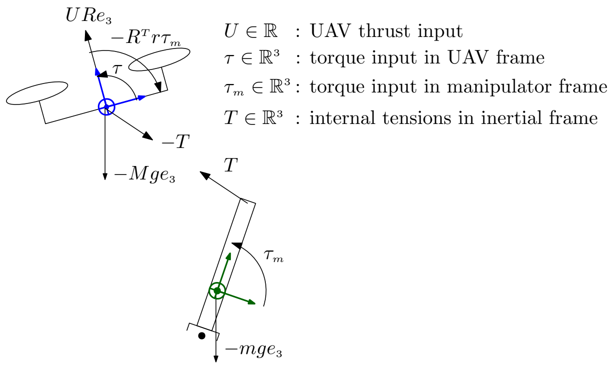

(b) Forces and torques applied on each rigid body.

Figure 2: Modeling of coupled UAV and manipulator, the two rigid bodies the system is composed of, with the real system illustrated in Fig. 1.

decompose a state and an input in the same way, namely

$$x \in \mathbb{X} :\Leftrightarrow (\mathcal{P}, \mathcal{V}) \in \mathbb{X} :\Leftrightarrow (p, r, P, R, v, \omega, V, \Omega) \in \mathbb{X}, \quad (4)$$

$$u \in \mathbb{U} := \mathbb{R}^7 :\Leftrightarrow (U, \tau, \tau_m) \in \mathbb{R} \times \mathbb{R}^3 \times \mathbb{R}^3. \quad (5)$$

Because we are interested in tracking problems for the system just described, we need a distance in the state space $\mathbb{X}$, namely, $d_{\mathbb{X}} : \mathbb{X} \times \mathbb{X} \to \mathbb{R}_{\geq 0}$, which we define as the Euclidean distance in $\mathbb{R}^{36}$ (as $\mathbb{X}$ is embedded in $\mathbb{R}^{36}$).

Given the state space $\mathbb{X}$ in (3), its tangent set at a point $x \in \mathbb{X}$ is given by

$$\begin{aligned} T_x\mathbb{X} := \big\{ &(\delta\mathcal{P}, \delta\mathcal{V}) \in T_{\mathcal{P}}\mathbb{SE}(3)^{\times 2} \times \mathbb{R}^{12} : \\ &\delta p + l\delta r e_3 - \delta P = 0_3, \\ &\delta v + l\delta r \mathcal{S}(\omega) e_3 + lr\mathcal{S}(\delta\omega) e_3 - \delta V = 0_3 \big\}, \end{aligned} \quad (7)$$

which is critical in computing the internal forces that allow the restrictions in (3) to be satisfied.

Before presenting the equations of motion, let us present first the net force and net torque applied on the manipulator (F_{net}^{man} and τ_{net}^{man}) and the UAV (F_{net}^{uav} and τ_{net}^{uav}), which are deduced by inspection of Fig. 2b. To be specific,

$$\begin{bmatrix} F_{net}^{man} \\ \tau_{net}^{man} \end{bmatrix} \equiv \begin{bmatrix} T(x,u) - mge_3 \\ \tau_m + l\mathcal{S}(e_3) r^T T(x,u) \end{bmatrix}, \quad (8a)$$

$$\begin{bmatrix} F_{net}^{uav} \\ \tau_{net}^{uav} \end{bmatrix} \equiv \begin{bmatrix} URe_3 - T(x,u) - Mge_3 \\ \tau - R^T r\tau_m \end{bmatrix}, \quad (8b)$$

with g as the acceleration due to gravity and where the internal tension forces $T : \mathbb{X} \times \mathbb{U} \to \mathbb{R}^3$ (expressed in the inertial frame) are given in (6a)[2].

We can now finally present the equations of motion. Given an appropriate input $u : \mathbb{R}_{\geq 0} \to \mathbb{U}$, a system's trajectory $x : \mathbb{R}_{\geq 0} \to \mathbb{X}$ evolves according to

$$\dot{x}(t) = X(x(t), u(t)) \text{ with } x(0) \in \mathbb{X}, \quad (9a)$$

where the vector field X is given by

$$X : \mathbb{X} \times \mathbb{U} \ni (x,u) \mapsto X(x,u) \in T_x\mathbb{X} \quad (9b)$$

$$X(x,u) := \begin{bmatrix} \dot{\mathcal{P}} \\ \dot{\mathcal{V}} \end{bmatrix} = \begin{bmatrix} \text{kinematics} \\ \text{dynamics} \end{bmatrix},$$

where the kinematics $\dot{\mathcal{P}}$ are given by

$$\begin{bmatrix} \dot{p} \\ \dot{r} \\ \dot{P} \\ \dot{R} \end{bmatrix} = \begin{bmatrix} v \\ r\mathcal{S}(\omega) \\ V \\ R\mathcal{S}(\Omega) \end{bmatrix}, \quad (10)$$

and the dynamics $\dot{\mathcal{V}}$ are given by (the dynamics are those of rigid-bodies where the net wrenches in (8) are applied)

$$\begin{bmatrix} \dot{v} \\ \dot{\omega} \\ \dot{V} \\ \dot{\Omega} \end{bmatrix} = \begin{bmatrix} \frac{1}{m}(T(x,u) - mge_3) \\ j^{-1}(\tau_m + l\mathcal{S}(e_3) r^T T(x,u) - \mathcal{S}(\omega) j\omega) \\ \frac{1}{M}(URe_3 - T(x,u) - Mge_3) \\ J^{-1}(\tau - R^T r\tau_m - \mathcal{S}(\Omega) J\Omega) \end{bmatrix} \quad (11)$$

$$\overset{(1)}{=} \begin{bmatrix} \frac{1}{m}(T(x,u) - mge_3) \\ j^{-1}\tau_m + \frac{l\mathcal{S}(e_3) r^T T(x,u)}{j_{xy}} + \left(\frac{j_{zz}}{j_{xy}} - 1\right) e_3^T\omega\mathcal{S}(e_3)\omega \\ \frac{1}{M}(URe_3 - T(x,u) - Mge_3) \\ J^{-1}(\tau - R^T r\tau_m - \mathcal{S}(\Omega) J\Omega) \end{bmatrix}.$$

[2] In (6b), we introduce the adimensional constant γ and, at this point, we emphasize only that $\gamma = 1$ when the manipulator is taken as a point-mass.

The vector field X in (9b) is composed of the system kinematics and dynamics. The system kinematics are given by the kinematics of each individual rigid body, in this particular case of the UAV and of the manipulator. On the other hand, the system dynamics are given by the linear and angular accelerations of each individual rigid body, by considering the net force (expressed in the inertial frame) and the net torque (expressed in the respective body frame) applied on each rigid body. The forces and torques contributing to the net force and net torque of each rigid body are visualized in Fig. 2b and presented in (8). It may be useful to discuss the net wrenches applied to each rigid body. The tension forces ($T(x,u) \in \mathbb{R}^3$ in (6a), expressed in the inertial frame) are internal forces, forming an action-reaction pair, and thus explaining its positive contribution to the manipulator's linear acceleration and its negative contribution to the UAV's. The manipulator input torque (τ_m expressed in the manipulator frame) also forms an action-reaction pair, thus explaining its positive contribution to the manipulator's angular acceleration and its negative contribution to the UAV's (in the UAV's orientation frame, the manipulator input torque is given by $-R^T r\tau_m$).

The tension forces ($T(x,u) \in \mathbb{R}^3$) constitute internal forces to the system, and the Newton-Euler's equations of motion do not provide any insight into these forces. However, the constraint that the state must remain in the state space $\mathbb{X}$ in (3), enforces the vector field X in (9b) to be in the tangent set of that set. This constraint uniquely defines the tensions, i.e., for any $(x,u) \in \mathbb{X} \times \mathbb{U}$,

$$X(x,u) \in T_x\mathbb{X} \Rightarrow T(x,u) \text{ as in (6a)}.$$

The Euler-Lagrange formalism provides an alternative, but equivalent, approach for obtaining the vector field in (9b).

Proposition 1. *The rotation of the manipulator around its axis of axial symmetry (third axis), along a solution* $t \mapsto x(t)$ *of* (9a)*, is given by* $t \mapsto e_3^T\omega(t) = e_3^T\omega(0)$ *if* $t \mapsto e_3^T\tau_m(t) = 0$.

Proof 2. *For convenience, define the function* $f : \mathbb{X} \to \mathbb{R}$, $f(x) := e_3^T\omega$. *Then, for any* $(x,u) \in \mathbb{X}\times\mathbb{U}$, $Df(x)X(x,u) = e_3^T j^{-1}(\tau_m + l\mathcal{S}(e_3) T(x,u) - \mathcal{S}(\omega) j\omega) = \frac{e_3^T\tau_m}{j_{zz}}$*, which concludes the proof.*

Proposition 1 implies that, if $e_3^T\tau_m = 0$, the rotation of the manipulator around its axis of symmetry remains constant along solutions. One could, at this point, assume that the rotation around that axis is non-existing at the initial time instant; however, we shall make that assumption only in one of the problems treated in this manuscript (for the UAV-slung-manipulator system, that we describe next).

Proposition 3. *If the UAV has axial symmetry around its third axis, then the vector field* X *in* (9b) *is invariant to rotations of the manipulator around its third axis (the axis of axial symmetry) and to rotations of the UAV around its third axis (the thrust axis).*

$$T(x,u) := \frac{1}{\gamma} r \left(\left(\frac{j_{xy}}{ml^2} I_3 + \frac{M}{m+M} e_3 e_3^T \right) \left(\frac{m}{M} U r^T R e_3 + m l \omega^T \Pi(e_3) \omega e_3 \right) + \frac{1}{l} \left(\mathcal{S}(e_3) \tau_m - j_{zz} e_3^T \omega \Pi(e_3) \omega \right) \right) \tag{6a}$$

$$\gamma \equiv 1 + \frac{j_{xy}}{ml^2} \frac{m+M}{M} \tag{6b}$$

A proof is found in [39]. Proposition 3 implies that the dynamics do not *see* rotations of the rigid bodies around their third axes. This motivates us to control the space orthogonal to the manipulator's third axis and the UAV's third axis as separate problems. Loosely speaking, we can treat the yaw motion of the manipulator and of the UAV as separate problems: the yaw motion of the UAV can be understood from Re_1, Re_2 and $e_3^T \Omega$; similarly, the yaw motion of the manipulator can be understood from re_1, re_2 and $e_3^T \omega$.

Invariance to rotations around the third axes also motivates us to introduce an equivalence relation in the set $\mathbb{X}$ in (3). To be specific, consider two states in $\mathbb{X}$, namely $x_1 \in \mathbb{X}$ and $x_2 \in \mathbb{X}$; then we define the relation $\sim$ as (below $R_3(\theta) := I_3 + \sin(\theta)\mathcal{S}(e_3) + (\cos(\theta) - 1)\Pi(e_3)$)

$$x_1 \sim x_2 :\Leftrightarrow \tag{12}$$

$$\begin{bmatrix} p_1 \\ r_1 \\ P_1 \\ R_1 \end{bmatrix} = \begin{bmatrix} p_2 \\ r_2 R_3(\theta) \\ P_2 \\ R_2 R_3(\Theta) \end{bmatrix}, \begin{bmatrix} v_1 \\ \omega_1 \\ V_1 \\ \Omega_1 \end{bmatrix} = \begin{bmatrix} v_2 \\ R_3^T(\theta)(\omega_2 + b e_3) \\ V_2 \\ R_3^T(\Theta)(\Omega_2 + B e_3) \end{bmatrix},$$

for some real θ, Θ, b and B; i.e., two states are equivalent up to rotations around their third axes and up to the third component of their body-frame angular-velocities. One can verify that the relation (12) is reflexive, symmetric and transitive, which supports the following result.

Proposition 4. *The relation defined in* (12) *is an equivalence relation in* $\mathbb{X}$.

Proposition (4) implies that the equivalence relation $\sim$ in (12) induces a quotient set, namely

$$\mathbb{X}\backslash_\sim := \{[x] : x \in \mathbb{X}\}, \tag{13}$$

where $[x] := \{x' \in \mathbb{X} : x' \sim x\}$ denotes the equivalence class associated to some $x \in \mathbb{X}$. We will require the quotient set later, which is the reason why we introduce it at this point. Also, it follows that the quotient set $\mathbb{X}\backslash_\sim$ can inherit the distance $d_{\mathbb{X}}$, i.e., we can define $d_{\mathbb{X}\backslash_\sim} : \mathbb{X}\backslash_\sim \times \mathbb{X}\backslash_\sim \to \mathbb{R}_{\geq 0}$ as

$$d_{\mathbb{X}\backslash_\sim}([x^1],[x^2]) := d_{\mathbb{X}}(x^1, x^2), \tag{14}$$

and where we note that the distance $d_{\mathbb{X}\backslash_\sim}$ in (14) is indeed well-defined [39], since the standard distance in $\mathbb{SO}(3)$ is insensitive to rotation of its arguments.

We consider two separate problems – see Fig. 3 – on the system just described: in the first we consider the manipulator torque input to be available, while in the second we restrict that torque input to be zero.

3.1. UAV-manipulator system

Hereafter, we refer to *UAV-manipulator system* when considering the manipulator torque input is available. With Fig. 3a in mind, we can then formulate the first problem treated in this paper, which is one of semi-pose tracking:

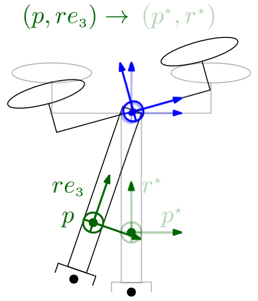

(a) Semi-pose tracking problem for *UAV-manipulator system*: desired semi-pose trajectory $(p^\star, r^\star)$ determines the whole state equilibrium in transparent; i.e., the system is differentially flat w.r.t. (p, re_3).

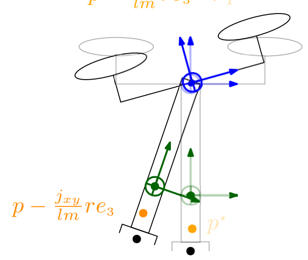

(b) Position tracking problem for *UAV-slung-manipulator system*: desired position trajectory $p^\star$ determines the whole state equilibrium in transparent; i.e., the system is differentially flat w.r.t. $p - \frac{j_{xy}}{lm} re_3$.

Figure 3: Two problems: one where the manipulator torque τ_m is available – Fig. 3a; and one where it is not – Fig. 3b.

we require the manipulator's position to track a desired position trajectory, and the manipulator's axis of axial symmetry (re_3) to track a desired attitude trajectory. The space orthogonal to the manipulator axis of axial symmetry is ignored, for the reasons discussed after Proposition 1 (thus the semi-pose tracking rather than (full-)pose tracking).

Problem 1 (UAV-Manipulator). *Consider the vector field* X *in* (9b)*. Given a desired position trajectory and a desired orientation trajectory, i.e,*

$$p^\star : \mathbb{R}_{\geq 0} \ni t \mapsto p^\star(t) \in \mathbb{R}^3,$$
$$r^\star : \mathbb{R}_{\geq 0} \ni t \mapsto r^\star(t) \in \mathbb{S}^2,$$

design a control law

$$u^{cl} := (U^{cl}, \tau^{cl}, \tau_m^{cl}) : \mathbb{R}_{\geq 0} \times \mathbb{X} \to \mathbb{U},$$

such that $\lim_{t\to\infty}(p(t) - p^\star(t)) = 0_3$ *and* $\lim_{t\to\infty}(r(t)e_3 - r^\star(t)) = 0_3$ *along the solution* $\mathbb{R}_{\geq 0} \ni t \mapsto x(t) \in \mathbb{X}$ *of* $\dot{x}(t) = X(x(t), u^{cl}(t, x(t)))$ *with* $x(0) \in \mathbb{X}_0$ *for some* $\mathbb{X}_0 \subset \mathbb{X}$.

Remark 5. *The problem treated here is a generalization of that treated in [38]. In [38], the manipulator is treated* *as a point-mass and only the kinematics of the UAV's attitude are considered. The vector field presented there is in fact recovered as follows: since the constraints in* (3) *must be satisfied, one imposes that* $re_3 = \frac{P-p}{l}$ *and that* $r\omega = \mathcal{S}\left(\frac{P-p}{l}\right)\frac{V-v}{l}$*; since the manipulator is taken as a point mass (and thus has no angular position and angular velocity, i.e.,* r *and* ω*), the manipulator's attitude equations (*$\dot{r}$ *in* (10) *and* $\dot{\omega}$ *in* (11)*) are ignored; finally, the internal forces are found by taking the limit when the moment of inertia of the manipulator vanishes, i.e., when* $j \to 0_{3\times3} \overset{(1)}{\Leftrightarrow} (j_{xy}, j_{zz}) \to (0,0)$ *[39].*

3.2. UAV-slung-manipulator system

Hereafter, we refer to *UAV-slung-manipulator system* when considering that the manipulator torque input is not available (Remark 6 sheds some light into the name *UAV-slung-manipulator system*). With some abuse of notation, and without hindering comprehension, when referring to the UAV-slung-manipulator system, we reuse and redefine the input u and the vector field X; to be specific, instead of the input in (5), we redefine it as

$$u \in \mathbb{U} := \mathbb{R}^4 :\Leftrightarrow (U, \tau) \in \mathbb{R} \times \mathbb{R}^3,$$

and, instead of the vector field in (9b), we redefine it as

$$X : \mathbb{X} \times \mathbb{U} \ni (x, u) \mapsto X(x, u) \in T_x\mathbb{X}$$
$$X(x, u) := X(x, (U, \tau, 0_3))|_{X \text{ in (9b)}}. \tag{15}$$

With Fig. 3b in mind, we can then formulate the second problem treated in this paper, which is one of position tracking: we require a specific point along the manipulator's axis of axial symmetry to track a desired position trajectory.

Problem 2 (UAV-slung-manipulator). *Consider the vector field* X *in* (15)*. Given a desired position trajectory, i.e,*

$$p^\star : \mathbb{R}_{\geq 0} \ni t \mapsto p^\star(t) \in \mathbb{R}^3,$$

design a control law

$$u^{cl} := (U^{cl}, \tau^{cl}) : \mathbb{R}_{\geq 0} \times \mathbb{X} \to \mathbb{U}$$

such that $\lim_{t\to\infty}(p(t) - \frac{j_{xy}}{lm} r(t)e_3 - p^\star(t)) = 0_3$ *along a solution* $\mathbb{R}_{\geq 0} \ni t \mapsto x(t) \in \mathbb{X}$ *of* $\dot{x}(t) = X(x(t), u^{cl}(t, x(t)))$ *with* $x(0) \in \mathbb{X}_0$ *for some* $\mathbb{X}_0 \subset \mathbb{X}$.

Remark 6. *The problem treated here is a generalization of that treated in [49], which deals with the slung-load problem. In [49], the UAV is tethered to a point mass, which is the system here described if we take the manipulator to be a point-mass. The vector field presented there is in fact recovered following the exact same procedure as in Remark 5.*

Remark 7. *In Problem 2, rather than requiring the manipulator's position* p *to track the desired trajectory, we require another position along the manipulator's axis of axial symmetry (*$p - \frac{j_{xy}}{lm} re_3$*) to track the desired trajectory (note however that those positions coincide when the manipulator is taken as a point mass, i.e., when* $j_{xy} = 0$*). The intuition for why* the center-of-mass position is not a flat output for a rod-like object with a non-zero moment inertia *is the same intuition for why* the position of the UAV is not a flat output for a UAV with a cable suspended load. *For a UAV with a cable suspended load, fixing the UAV's position allows for the load to oscillate (like a pendulum with the UAV as a pivot point) while fixing the load's position fixes the UAV's position. Also, the intuitive idea is that a rod-like object with length* l *and moment of inertia* j_{xy} *is "equal" to a rod-like object with length* $l + \frac{j_{xy}}{lm}$ *and no moment of inertia.*

Remark 8. *Notice that Problem 1 describes a semi-pose tracking problem, while Problem 2 describes a position tracking problem. This difference stems from the fact that the UAV-slung-manipulator system is deprived of the manipulator torque input, which prevents the manipulator pose from tracking an arbitrary pose. In fact, as we verify later, for the UAV-slung-manipulator system, the desired position trajectory* $p^\star$ *in Problem 2 imposes a desired semi-pose trajectory (this is verified by means of differential flatness).*

4. Control strategy summary

In this section, we explain the pursued control strategy, illustrated in Fig. 4. The strategy is composed of three steps, which we explain next. The specifics of these three steps are different when solving Problems 1 and 2, but the overall idea behind them is the same.

Recall then Proposition 3, which states that rotations around the rigid bodies' third axes may be ignored. Our first step is to design a bijective mapping (the specific mapping f and the codomain $\mathbb{Y}$ are specific to Problem 1 and 2, and are provided later)

$$f : \mathbb{X}\backslash_\sim \ni [x] \mapsto f([x]) =: y \in \mathbb{Y} \tag{16}$$

which "reorders" the state in a manner that highlights the hierarchical/cascaded structure of the problem, while ignoring the rotations around the rigid bodies third axes: the necessity of the equivalence relation $\sim$ in (12) and of the quotient set $\mathbb{X}\backslash_\sim$ in (13) becomes clear at this point. This step is called state transformation – see Fig. 4.

In our second step, we design a control law

$$\bar{u}^{cl}_x : \mathbb{U} \ni v \mapsto \bar{u}^{cl}_x(v) \in \mathbb{U} \tag{17}$$

which transforms the input (from v to u – see input transformation in Fig. 4), in such a way that when we compose this input transformation and state transformation with the system dynamics, we obtain the transformed dynamics in $\mathbb{Y}$, i.e.,

$$Y : \mathbb{Y} \times \mathbb{U} \ni (y, v) \mapsto Y(y, v) \in T_y\mathbb{Y} \tag{18}$$
$$Y(y, v) := Df([x])X(x, \bar{u}^{cl}_x(v))|_{x\in f^{-1}(y)} (= \dot{y}),$$

where we emphasize that f^{-1} exists since the map f is invertible. Let us emphasize some key points regarding the input transformation $\bar{u}^{cl}_x$ in (17) and the vector field Y in (18). *(a)* The input transformation $\bar{u}^{cl}_x$ is designed so as to make explicit the cascaded structure of the vector field Y (one may think of Y as a chain of integrators). *(b)* We (must) show that the vector field Y in (18) is well defined, in the sense that (18) is independent of the choice of the representative belonging the equivalence class $f^{-1}(y)$

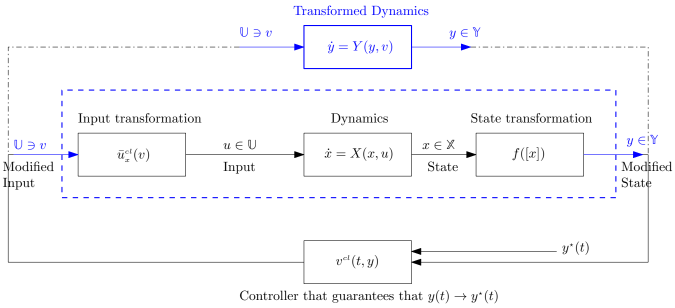

Figure 4: Control strategy block-diagram.

(notice that for any $y \in \mathbb{Y}$, $f^{-1}(y)$ is an equivalence class, i.e., $f^{-1}(y) \in \mathbb{X}\backslash_\sim$). *(c)* The vector field Y is in a form for which controllers are already available.

In the third and final step, we analyze differential flatness properties of the vector field Y, and, based on that, determine the equilibrium (more precisely the equilibria)

$$y^\star : \mathbb{R} \ni t \mapsto y^\star(t) \in \mathbb{Y}$$

for which it is guaranteed that Problems 1 and 2 are satisfied. Finally, since the vector field Y is in a form for which controllers are already available, we recruit a control law from the literature

$$v^{cl} : \mathbb{R} \times \mathbb{Y} \ni (t, y) \mapsto v^{cl}(t, y) \in \mathbb{U} \tag{19}$$

that guarantees that a solution $t \mapsto y(t)$, of the differential equation $\dot{y}(t) = Y(y(t), v^{cl}(t, y(t)))$, tracks the desired equilibrium $t \mapsto y^\star(t)$. Problems 1 and 2 are then accomplished if one composes the input transformation $\bar{u}_x^{cl}$ in (17) with the control law v^{cl} in (19), i.e.,

$$\begin{aligned} &u^{cl} : \mathbb{R} \times \mathbb{X} \to \mathbb{U} \\ &u^{cl}(t, x) := \bar{u}_x^{cl}(v^{cl}(t, f([x]))). \end{aligned} \tag{20}$$

Remark 9. *If $f : \mathbb{X} \to \mathbb{Y}$ provided a bijection from $\mathbb{X}$ to $\mathbb{Y}$, or, in other words, a coordinate change from $\mathbb{X}$ to $\mathbb{Y}$, then,* (18) *would read as*

$$Y(y, v) := Df(x)X(x, \bar{u}_x^{cl}(v)|_{x=f^{-1}(y)} (= \dot{y}),$$

which is the standard equation for computing the vector field in the new coordinates in $\mathbb{Y}$.

Let us now look at each Problem individually.

5. UAV-manipulator problem

We verify next that the UAV-manipulator system behaves as two decoupled systems, as illustrated in Fig. 5: one thrust-propelled system by considering the motion of the center-of-mass of the whole system; and one unit vector double integrator system corresponding to the attitude dynamics of the manipulator. The three steps we follow next have been described in the previous section.

5.1. State transformation

Recall the discussion from Section 4. Let us then introduce the set $\mathbb{Y}$ as

$$\mathbb{Y} = \mathbb{Y}_1 \times \mathbb{Y}_2 \tag{21a}$$

$$\mathbb{Y}_1 := \{(p_{cm}, v_{cm}, n, \varpi) \in (\mathbb{R}^3)^4 : n^T n = 1, n^T \varpi = 0\}, \tag{21b}$$

$$\mathbb{Y}_2 := \{(r, \omega) \in (\mathbb{R}^3)^2 : r^T r = 1, r^T \omega = 0\}, \tag{21c}$$

with the inherited distances $d_{\mathbb{Y}_1} := d_{\mathbb{R}^{12}}$, $d_{\mathbb{Y}_2} := d_{\mathbb{R}^6}$ and $d_{\mathbb{Y}} := d_{\mathbb{R}^{18}}$. The set $\mathbb{Y}_1$ will be used for the subsystem that behaves as a thrust-propelled system; while the set $\mathbb{Y}_2$ will be used for the subsystem that behaves as a unit vector double integrator system (see Fig. 5). Hereafter, and for convenience, we decompose elements in the sets above as

$$y \in \mathbb{Y} :\Leftrightarrow (y_1, y_2) \in \mathbb{Y}_1 \times \mathbb{Y}_2, \tag{22a}$$

$$y_1 \in \mathbb{Y}_1 :\Leftrightarrow (p_{cm}, v_{cm}, n, \varpi) \in \mathbb{Y}_1, \tag{22b}$$

$$y_2 \in \mathbb{Y}_2 :\Leftrightarrow (r, \omega) \in \mathbb{Y}_2. \tag{22c}$$

Hereafter, we denote as well

$$v \in \mathbb{U} :\Leftrightarrow (v_1, v_2) \in \mathbb{R}^4 \times \mathbb{R}^3, \tag{23a}$$

$$v_1 \in \mathbb{R}^4 :\Leftrightarrow (U, \tau) \in \mathbb{R} \times \mathbb{R}^3, \tag{23b}$$

$$v_2 \in \mathbb{R}^3 :\Leftrightarrow \tau_m \in \mathbb{R}^3, \tag{23c}$$

where v_1 will be the input to one subsystem (thrust propelled), and v_2 will be the input to the other subsystem (unit vector double integrator).

Based on Fig. 5, consider then the mapping

$$f : \mathbb{X}\backslash_\sim \ni [x] \mapsto f([x]) \in \mathbb{Y} \tag{24a}$$

$$f([x]) := \begin{bmatrix} \frac{mp+MP}{m+M} \\ \frac{mv+MV}{m+M} \\ Re_3 \\ \Pi(Re_3) R\Omega \\ \hdashline re_3 \\ \Pi(re_3) r\omega \end{bmatrix} \left(= \begin{bmatrix} p_{cm} \\ v_{cm} \\ n \\ \varpi \\ \hdashline r \\ \omega \end{bmatrix} = \begin{bmatrix} y_1 \\ \hdashline y_2 \end{bmatrix} \right),$$

with $\mathbb{Y}$ in (21a), and consider as well the mapping

$$h : \mathbb{Y} \ni y \mapsto h(y) \in \mathbb{X}\backslash_\sim \tag{24b}$$

$$h(y) := \underbrace{\begin{bmatrix} p_{cm} - l\frac{M}{m+M} r \\ \bar{r} \\ p_{cm} + l\frac{m}{m+M} r \\ \bar{R} \\ v_{cm} - l\frac{M}{m+M} \mathcal{S}(\omega) r \\ \bar{r}^T \omega \\ v_{cm} + l\frac{m}{m+M} \mathcal{S}(\omega) r \\ \bar{R}^T \varpi \end{bmatrix}}_{\substack{\text{where } \bar{r} \in \mathbb{SO}(3) \text{ is s.t. } \bar{r}e_3 = r \\ \text{where } \bar{R} \in \mathbb{SO}(3) \text{ is s.t. } \bar{R}e_3 = n}} \left(= \begin{bmatrix} p \\ r \\ P \\ R \\ \hdashline v \\ \omega \\ V \\ \Omega \end{bmatrix} = [x] \right),$$

where $[\cdot]$ above denotes the equivalence class as defined immediately after (13).

Proposition 10. *The map f in* (24a) *is well defined, and*

$$f \circ h = id_{\mathbb{Y}} \text{ and } h \circ f = id_{\mathbb{X}\backslash_\sim}, \tag{25}$$

i.e., $h = f^{-1}$ and $f = h^{-1}$.

Proof 11. *The map f in* (24a) *is defined with a representative of an equivalence class, so we must show that f is independent of the choice of representative. Notice that (below $R_3(\theta) := I_3 + \sin(\theta)\mathcal{S}(e_3) + (\cos(\theta) - 1)\Pi(e_3)$)*

$$Re_3 = (RR_3(\theta))e_3, \text{ and that}$$

$$\Pi(Re_3) R\Omega = \Pi((RR_3(\theta))e_3)(RR_3(\theta))(R_3^T(\theta)(\Omega + Be_3)),$$

which suffices to conclude that f is independent of the choice of representative belonging to an equivalence class

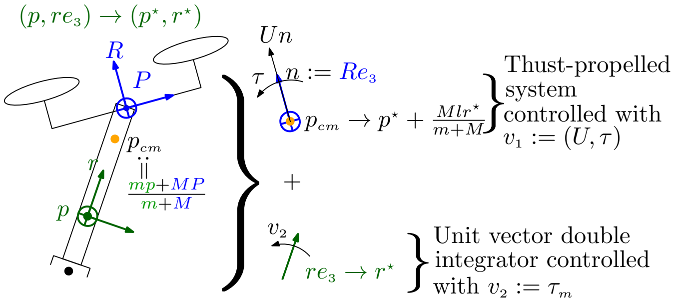

Figure 5: By means of appropriate state and input transformations, the UAV-manipulator may be understood as two decoupled systems: one thrust-propelled system and one unit-vector double-integrator system.

established by the equivalence relation in (12) *(i.e., for any* $x \in \mathbb{X}$ *and for any* $\bar{x}, \tilde{x} \in [x] \in \mathbb{X}\backslash_\sim$, $f([\bar{x}]) = f([\tilde{x}])$*). The second part of the Proposition follows from straightforward computations. Let us just illustrate the identities in* (25) *for the component* ϖ *of* f *(denote it* $f|_\varpi$*) and the component* Ω *of* h *(denote it* $h|_\Omega$*) – i.e., we verify that* $f|_\varpi \circ h(y) = \varpi$ *and that* $h|_\Omega \circ f([x]) = [\Omega]$ *(where, by the equivalence relation in* (12)*, angular velocities are equivalent up to rotations around the third body axis and up to the third-component – i.e.,* $[\Omega] := [R_3(\Theta)(\Omega + Be_3)]$ *for any real* Θ *and* B*). Then, notice that*

$$
\begin{aligned}
f|_\varpi \circ h(y) &= f|_\varpi(h(y)) \overset{(24a)}{\equiv} \Pi\left(Re_3\right) R\Omega|_{R \text{ and } \Omega \text{ as in } (24b)} \\
&= \Pi\left(\bar{R}e_3\right)\bar{R}\bar{R}^T\varpi = \Pi\left(\bar{R}e_3\right)\varpi \\
{}_{(24b):\bar{R}e_3 = n} &= \Pi\left(n\right)\varpi = (I_3 - nn^T)\varpi \\
{}_{(22):n^T\varpi = 0} &= \varpi.
\end{aligned}
$$

Finally, notice that

$$
\begin{aligned}
h|_\Omega \circ f([x]) &= h|_\Omega(f([x])) \overset{(24b)}{\equiv} [\bar{R}^T\varpi]|_{\varpi \text{ as in } (24a)} \\
&= [\bar{R}^T\Pi\left(Re_3\right)R\Omega] = [\bar{R}^T R\Pi\left(e_3\right)\Omega] \\
{}_{Re_3 \overset{(24a)}{=} n \overset{(24b)}{=} \bar{R}e_3 \Rightarrow \Rightarrow \bar{R}^T R = R_3^T(\Theta)} &= [R_3^T(\Theta)\Pi\left(e_3\right)\Omega] \\
{}_{(12)} &= [\Pi\left(e_3\right)\Omega] = [\Omega - \Omega^T e_3 e_3] = [\Omega].
\end{aligned}
$$

5.2. Input transformation and transformed vector field

Let us construct the input transformation in two steps. For that purpose, consider the transformed dynamics with the original input (not the transformed input), which are given by

$$
\dot{y} = Df([x])X(x, u) \Leftrightarrow \tag{27}
$$

$$
\begin{bmatrix} \dot{p}_{cm} \\ \dot{v}_{cm} \\ \dot{n} \\ \dot{\varpi} \\ \hline \dot{r} \\ \dot{\omega} \end{bmatrix} = \begin{bmatrix} \frac{mv+MV}{m+M} \\ \frac{U}{m+M}Re_3 - ge_3 \\ \mathcal{S}\left(\Pi\left(Re_3\right)R\Omega\right)Re_3 \\ \Pi\left(Re_3\right)R(\star_1) \\ \hline \mathcal{S}\left(\Pi\left(re_3\right)r\omega\right)re_3 \\ \Pi\left(re_3\right)(\star_2) \end{bmatrix}, \text{ where}
$$

$$
(\star_1) = J^{-1}(\tau - R^T r\tau_m - \mathcal{S}\left(\Omega\right)J\Omega) - e_3^T\Omega\mathcal{S}\left(\Omega\right)e_3,
$$

$$
(\star_2) = \frac{m+M}{l^2 mM}\frac{1}{\gamma}\left(\tau_m + \mathcal{S}\left(e_3\right)\left(\frac{mlU}{m+M}r^T Re_3 + j_{zz}e_3^T\omega\omega\right)\right).
$$

If follows from (27) that the original input $u = (U, \tau, \tau_m)$ has the effects illustrated in Fig. 6. (i) The UAV torque input τ only makes the UAV rotate (not the manipulator). (ii) The manipulator torque input τ_m makes the manipulator rotate, but it also makes the UAV rotate (in an opposite direction, and with a different scaling – factor $\|J^{-1}R^T r\| = \|J^{-1}\|$ in $\star_1$ and factor $\frac{m+M}{l^2 mM}\frac{1}{\gamma}$ in $\star_2$). (iii) The UAV thrust input U makes the whole system (i.e., its center-of-mass) accelerate along the UAV's third body axis; but it also produces a torque on the manipulator third axis, which makes it rotate. The previous discussion provides the basis for the design of the input transformation, whose idea is to design a UAV torque input τ that controls the UAV attitude by canceling the effect of the manipulator torque input τ_m on the UAV attitude; and next, to design a manipulator torque input τ_m that controls the manipulator attitude by canceling the effect of the UAV thrust input U on the manipulator's attitude (notice the design is made in a cascaded fashion). Given some $x \in \mathbb{X}$ and some $\tau_\psi \in \mathbb{R}$, consider then

$$
\bar{u}_{1,x}^{cl} : \mathbb{U} \to \mathbb{U} \tag{28a}
$$

$$
\bar{u}_{1,x}^{cl}(u) := \begin{bmatrix} (m+M)U \\ \left\{ \begin{matrix} J(\Pi(e_3)R^T\tau + \tau_\psi e_3 + e_3^T\Omega\mathcal{S}(\Omega)e_3) + \\ +R^T r\tau_m + \mathcal{S}(\Omega)J\Omega \end{matrix} \right\} \\ \tau_m \end{bmatrix}
$$

which when composed with (27) yields $\dot{v}_{cm} = URe_3 - ge_3$ and $\dot{\varpi} = \Pi\left(Re_3\right)\tau$ (for the purpose of τ_ψ in (28a), we ask the reader to await until Remark 13). Then consider

$$
\bar{u}_{2,x}^{cl} : \mathbb{U} \to \mathbb{U} \tag{28b}
$$

$$
\bar{u}_{2,x}^{cl}(u) := \begin{bmatrix} U \\ \tau \\ \left\{ \begin{matrix} \frac{l^2 mM}{m+M}\gamma\Pi(e_3)r^T\tau_m - \\ -\mathcal{S}(e_3)\left(mlUr^T Re_3 + j_{zz}e_3^T\omega\omega\right) \end{matrix} \right\} \end{bmatrix}
$$

which when composed with (27) (and after applying (28a) first) it leads to $\dot{\omega} = \Pi\left(re_3\right)\tau_m$.

Consider then the input transformation as a composition of the previous control laws (28a) and (28b), i.e.,

$$
\begin{aligned}
&\bar{u}_x^{cl} : \mathbb{U} \to \mathbb{U} \\
&\bar{u}_x^{cl}(u) := \bar{u}_{1,x}^{cl} \circ \bar{u}_{2,x}^{cl}(u).
\end{aligned} \tag{28c}
$$

Given the input transformation in (28c) and the state transformation in (24a), one can then compute the transformed dynamics. In fact, it follows that composing (27) with the control law (28c) results in

$$
\dot{y} = Df([x])X(x, \bar{u}_x^{cl}(u)) \Leftrightarrow
$$

$$
\begin{bmatrix} \dot{p}_{cm} \\ \dot{v}_{cm} \\ \dot{n} \\ \dot{\varpi} \\ \hline \dot{r} \\ \dot{\omega} \end{bmatrix} = \begin{bmatrix} \frac{mv+MV}{m+M} \\ URe_3 - ge_3 \\ \mathcal{S}\left(\Pi\left(Re_3\right)R\Omega\right)Re_3 \\ \Pi\left(Re_3\right)\tau \\ \hline \mathcal{S}\left(\Pi\left(re_3\right)r\omega\right)re_3 \\ \Pi\left(re_3\right)\tau_m \end{bmatrix}
$$

and, as such, the vector field in the new coordinates $Y : \mathbb{Y} \times \mathbb{U} \ni (y, v) \mapsto Y(y, v) \in T_y\mathbb{Y}$ is given by

$$
Y(y, v) := Df([x])X(x, \bar{u}_x^{cl}(v))|_{x \in h(y)} \tag{29}
$$

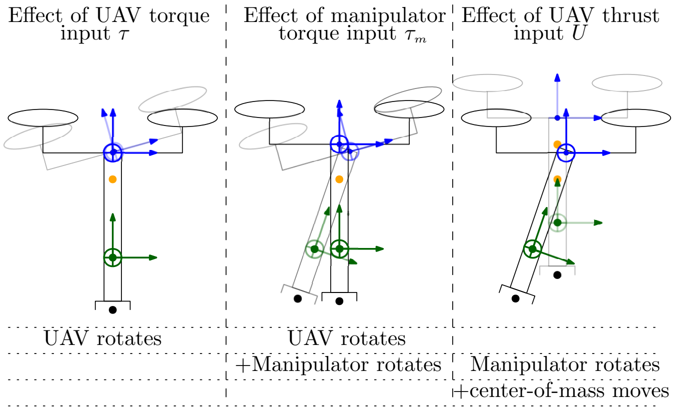

Figure 6: Effects of original input $u = (U, \tau, \tau_m)$ in UAV-manipulator system. These effects follow from the dynamics equations in (11), and, for brevity, we discuss only the effect of U in $\dot{\omega}$: from (11), the manipulator's angular acceleration is given by $j\dot{\omega} + \mathcal{S}(\omega)j\omega = \tau_m + l\mathcal{S}(e_3)r^T T(x,u)$, with the internal forces $T(x,u)$ in (6a); it then follows that the UAV thrust input U has a contribution to the change of the manipulator's angular velocity ω.

$$\begin{bmatrix} \dot{y}_1 \\ \hline \dot{y}_2 \end{bmatrix} = \begin{bmatrix} Y_1(y_1, v_1) \\ \hline Y_2(y_2, v_2) \end{bmatrix} = \begin{bmatrix} v_{cm} \\ Un - ge_3 \\ \mathcal{S}(\varpi)\, n \\ \Pi(n)\, \tau \\ \hline \mathcal{S}(\omega)\, r \\ \Pi(r)\, \tau_m \end{bmatrix} = \begin{bmatrix} \dot{p}_{cm} \\ \dot{v}_{cm} \\ \dot{n} \\ \dot{\varpi} \\ \hline \dot{r} \\ \dot{\omega} \end{bmatrix},$$

and where we draw attention to the state and input decompositions in (22) and (23). It is now clear that the UAV-manipulator system can be understood as two decoupled systems, with vectors fields Y_1 and Y_2 (and for which controllers are found in the literature). Let us highlight the cascaded structure of those two vector fields (below, $0 \equiv 0_{3\times 3}$ and $I \equiv I_3$), which is better understood if they are rewritten as

$$Y_1(y_1, v_1) = \begin{bmatrix} 0 & I & 0 & 0 \\ 0 & 0 & UI & 0 \\ 0 & 0 & 0 & -\mathcal{S}(n) \\ 0 & 0 & 0 & 0 \end{bmatrix} \begin{bmatrix} p_{cm} \\ v_{cm} \\ n \\ \varpi \end{bmatrix} + \begin{bmatrix} 0_3 \\ -ge_3 \\ 0_3 \\ \Pi(n)\, \tau \end{bmatrix}, \quad (30a)$$

$$Y_2(y_2, v_2) = \begin{bmatrix} 0 & -\mathcal{S}(r) \\ 0 & 0 \end{bmatrix} \begin{bmatrix} r \\ \omega \end{bmatrix} + \begin{bmatrix} 0_3 \\ \Pi(r)\, \tau_m \end{bmatrix}. \quad (30b)$$

Recall then Problem 1, and notice that the vector field Y_1 is concerned with the motion of the center-of-mass of the system, while the vector field Y_2 is concerned with the angular position motion of the manipulator. This motivates us to introduce the desired center-of-mass position based on the desired manipulator linear and angular positions ($p^\star$ and $r^\star$ in Problem 1), defined as

$$p^\star_{cm} : \mathbb{R} \to \mathbb{R}^3, p^\star_{cm}(t) := p^\star(t) + l\frac{M}{m+M} r^\star(t), \quad (31)$$

and which, for reasons made clear next, must satisfy

$$p^\star_{cm} \in \mathcal{C}^4, \quad (32a)$$

$$\inf_{t\in\mathbb{R}} \|p^{\star(2)}_{cm}(t) + ge_3\| > 0, \quad (32b)$$

$$\sup_{t\in\mathbb{R}} p^{\star(i)}_{cm}(t) < \infty \text{ for } i \in \{2,3,4\}. \quad (32c)$$

5.3. Differential flatness

Differential flatness with respect to the center-of-mass has been shown in [50], when considering the system's motion is constrained to a plane (two-dimensional setting). In this section, we reach the same conclusion while conducting instead our analysis in a three-dimensional setting.

It follows from the cascaded structure of the vector field Y_1 in (30a) that it is differentially flat with respect to the position of the center-of-mass. In fact, if we require $t \mapsto p_{cm}(t) := p^\star_{cm}(t)$, then we find two equilibria trajectories and two equilibria inputs, namely (below $y^\star_{1\pm}$ stands for the two solutions, namely $y^\star_{1+}$ and $y^\star_{1-}$)

$$y^\star_{1\pm} : \mathbb{R} \ni t \mapsto y^\star_{1\pm}(t) \in \mathbb{Y}_1 \quad (33a)$$

$$y^\star_{1\pm}(t) := \begin{bmatrix} p^\star_{cm}(t) \\ v^\star_{cm}(t) \\ n^\star_{\pm}(t) \\ \varpi^\star(t) \end{bmatrix} := \begin{bmatrix} p^{\star(0)}_{cm}(t) \\ p^{\star(1)}_{cm}(t) \\ \pm\frac{p^{\star(2)}_{cm}(t)+ge_3}{\|p^{\star(2)}_{cm}(t)+ge_3\|} \\ \mathcal{S}\left(\frac{p^{\star(2)}_{cm}(t)+ge_3}{\|p^{\star(2)}_{cm}(t)+ge_3\|}\right)\frac{p^{\star(3)}_{cm}(t)}{\|p^{\star(2)}_{cm}(t)+ge_3\|} \end{bmatrix},$$

and (below we use the definition of $\varpi^\star$ presented above)

$$v^\star_{1\pm} : \mathbb{R} \to \mathbb{R}^4, v^\star_{1\pm}(t) := \begin{bmatrix} \pm\|p^{\star(2)}_{cm}(t) + ge_3\| \\ \varpi^{\star(1)}(t) \end{bmatrix}. \quad (33b)$$

At this point, it becomes clear the necessity of the constraints (32a), (32b). Since (33a) and (33b) require $p^\star_{cm}$ to be four times continuously differentiable, (32a) becomes clear. On the other hand, $y^\star_{1\pm}$ is only well defined if (32b) is satisfied. The existence of two equilibria is also clear intuitively: loosely speaking, for $y^\star_{1+}$ the UAV points upwards and its thrust is positive, and for $y^\star_{1-}$ the UAV points downwards and its thrust is negative (regardless, in both cases, the center-of-mass tracks the desired trajectory).

Similarly, it follows from the cascaded structure of the vector field Y_2 in (30b) that it is differentially flat with respect to the angular position of the manipulator. In fact, if we require $t \mapsto r(t) := r^\star(t)$, then we find two equilibria trajectories and one equilibrium input, namely

$$y^\star_{2\pm} : \mathbb{R} \ni t \mapsto y^\star_{2\pm}(t) \in \mathbb{Y}_2 \quad (34a)$$

$$y^\star_{2\pm}(t) := \begin{bmatrix} r^\star_{\pm}(t) \\ \omega^\star(t) \end{bmatrix} := \begin{bmatrix} \pm r^{\star(0)}(t) \\ \mathcal{S}(r^{\star(0)}(t))\, r^{\star(1)}(t) \end{bmatrix}$$

and

$$\mathbb{R} \ni t \mapsto v^\star_2(t) := \mathcal{S}(r^{\star(0)}(t))\, r^{\star(2)}(t) \in \mathbb{R}^3. \quad (34b)$$

The equilibria $\{y^\star_{1+}, y^\star_{1-}\}$ and $\{y^\star_{2+}, y^\star_{2-}\}$ just defined allows us to compute four equilibria in the original system apart from rotations around the rigid bodies third axes; i.e., it allows us to compute four equilibria equivalence classes (which we denote by $\{[x]^\star_{+,+}, [x]^\star_{-,+}, [x]^\star_{+,-}, [x]^\star_{-,-}\}$), with the help of the map h in (24b), namely

$$[x]^\star_{\pm,\mp} : \mathbb{R} \ni t \mapsto [x]^\star_{\pm,\mp}(t) := h(y^\star_{\pm,\mp}(t)) \in \mathbb{X}\backslash_\sim, \quad (35)$$

$$y^\star_{\pm,\mp} : \mathbb{R} \ni t \mapsto y^\star_{\pm,\mp}(t) := (y^\star_{1\pm}(t), y^\star_{2\mp}(t)) \in \mathbb{Y}.$$

(Note that the first slot $\pm$ in $y^\star_{\pm,(\cdot)}$ is related to the equilibria $y^\star_{1\pm}$; and the second slot $\pm$ in $y^\star_{(\cdot),\pm}$ is related to the equilibria $y^\star_{2\pm}$.)

Assumption 12. *With the equilibria* $y^\star_{1\pm}$ *in* (33a) *and*

$y^\star_{2\pm}$ *in* (34a) *in mind, assume there exist controllers*

$$v_1^{cl} : \mathbb{R} \times \mathbb{Y}_1 \to \mathbb{R}^4, \quad v_2^{cl} : \mathbb{R} \times \mathbb{Y}_2 \to \mathbb{R}^3, \tag{36a}$$

that guarantee that along solutions of

$$\dot{y}_1(t) = Y_1(y_1(t), v_1^{cl}(t, y_1(t))), y_1(0) \in \mathbb{Y}_1,$$
$$\dot{y}_2(t) = Y_2(y_2(t), v_2^{cl}(t, y_2(t))), y_2(0) \in \mathbb{Y}_2,$$

it holds that

$$\lim_{t\to\infty}(y_1(t) - y^\star_{1+}(t)) = 0_{12} \text{ or } \lim_{t\to\infty}(y_1(t) - y^\star_{1-}(t)) = 0_{12},$$
$$\lim_{t\to\infty}(y_2(t) - y^\star_{2+}(t)) = 0_6 \text{ or } \lim_{t\to\infty}(y_2(t) - y^\star_{2-}(t)) = 0_6,$$

which in turn implies that

$$\lim_{t\to\infty}(p_{cm}(t) - p^\star_{cm}(t)) = 0_3,$$
$$\lim_{t\to\infty}(r(t) \pm r^\star(t)) = 0_3.$$

Assume as well that there exist non-empty $\mathbb{Y}_{1,0} \subset \mathbb{Y}_1$ *and* $\mathbb{Y}_{2,0} \subset \mathbb{Y}_2$ *such that along solutions of*

$$\dot{y}_1(t) = Y_1(y_1(t), v_1^{cl}(t, y_1(t))), y_1(0) \in \mathbb{Y}_{1,0},$$
$$\dot{y}_2(t) = Y_2(y_2(t), v_2^{cl}(t, y_2(t))), y_2(0) \in \mathbb{Y}_{2,0},$$

it holds that $y^\star_{1+}$ *and* $y^\star_{2+}$ *are stable, and that*

$$\lim_{t\to\infty}(y_1(t) - y^\star_{1+}(t)) = 0_{12}, \quad \lim_{t\to\infty}(y_2(t) - y^\star_{2+}(t)) = 0_6. \tag{36b}$$

Finally, assume that these controllers render the equilibria trajectories $y^\star_{1-}$ *and* $y^\star_{2-}$ *unstable.*

Note that the vector field Y_1 in (29) is that of a VTOL vehicle, and thus we are able to leverage controllers from the literature to control the position of the center-of-mass [41–45]. Similarly, the vector field Y_2 in (29) is that of a second order system in the unit sphere, and thus we are able to leverage controllers from the literature to control the attitude of the manipulator [46–48]. As such, Assumption 12 is indeed satisfied (provided that the desired center-of-mass position trajectory satisfies the constraints in (32)), and we can leverage controllers that are found in the literature and which satisfy the requirements described in Assumption 12.

Remark 13. *Define* $g : \mathbb{X} \ni x \mapsto g(x) := e_3^T\Omega \in \mathbb{R}$, *and notice that*

$$Dg(x)X(x, \bar{u}_x^{cl}(v)) = \tau_\psi$$

for any $(x, v, \tau_\psi) \in \mathbb{X}\times\mathbb{U}\times\mathbb{R}$. *As such, given some positive gain* $k > 0$, *consider the control law*

$$\tau_\psi^{cl} : \mathbb{R} \times \mathbb{X} \ni (t, x) \mapsto \tau_\psi^{cl}(t, x) \in \mathbb{R}$$
$$\tau_\psi^{cl}(t, x) := -kg(x) = -ke_3^T\Omega.$$

It then follows that, $t \mapsto e_3^T\dot{\Omega}(t) = -ke_3^T\Omega(t)$, *which implies that* $t \mapsto e_3^T\Omega(t) = e_3^T\Omega(0)e^{-kt}$ *along solutions of the closed loop system. For simplicity, we shall assume that the chosen control law for the UAV yaw motion is always the one shown above, which guarantees only that the UAV does not asymptotically spin around its third axis (loosely speaking, it does not yaw asymptotically). More complex control laws may be chosen for* τ^{cl}, *but none (including the one above) interferes with the motion of the equivalence class (i.e., with* $t \mapsto [x(t)]$*).*

Let us then present the result that guarantees that Problem 1 is indeed solved. For that purpose, let Assumption 12 be satisfied, and construct the control law in the original system as a composition of the input transformation $\bar{u}_x^{cl}$ in (28c) with the control laws presented in Assumption 12, i.e.,

$$u^{cl} : \mathbb{R} \times \mathbb{X} \ni (t, x) \mapsto u^{cl}(t, x) \in \mathbb{R}^7 \tag{37}$$
$$u^{cl}(t, x) = \bar{u}_x^{cl}(v^{cl}(t, y))|_{y=f([x])}$$
$$v^{cl}(t, y) := (v_1^{cl}(t, y_1), v_2^{cl}(t, y_2)),$$

which leads to the closed loop vector field

$$\mathbb{R}\times\mathbb{X} \ni (t, x) \mapsto X^{cl}(t, x) := X(x, u^{cl}(t, x)) \in T_x\mathbb{X}. \tag{38}$$

Theorem 14. *Consider the closed loop vector field* X^{cl} *in* (38)*, constructed under the assumption the controllers in Assumption 12 are provided. Then, along solutions of*

$$\dot{x}(t) = X^{cl}(t, x(t)), \text{ with } [x(0)] \in h(\mathbb{Y}_{1,0} \times \mathbb{Y}_{2,0}), \tag{39}$$

where $h(\mathbb{Y}_{1,0} \times \mathbb{Y}_{2,0}) := \{h(y) \in \mathbb{X}\backslash_\sim : y \in \mathbb{Y}_{1,0} \times \mathbb{Y}_{2,0}\}$, *it follows that*

$$\lim_{t\to\infty} d_{\mathbb{X}\backslash\sim}([x(t)], [x]^\star_{+,+}(t)) = 0, \tag{40}$$

where the equilibrium equivalence class $[x]^\star_{+,+}$ *is defined in* (35) *and the distance* $d_{\mathbb{X}\backslash\sim}$ *is defined in* (14)*; i.e., it follows that Problem 1 is satisfied.*

Proof 15. *Since* $[x(0)] \in h(\mathbb{Y}_{1,0} \times \mathbb{Y}_{2,0})$ *it follows that* $y(0) := f([x(0)]) \Rightarrow (y_1(0), y_2(0)) \in \mathbb{Y}_{1,0}\times\mathbb{Y}_{2,0}$*; moreover, if we apply the control law* (37)*, then* (36b) *in Assumption 12 holds, that is,* $\lim_{t\to\infty}\big(y(t) - y^\star_{+,+}(t)\big)$*. Finally, because* $t \mapsto y(t) = f([x(t)]) \Leftrightarrow t \mapsto [x(t)] = h(y(t))$*, it follows that* $\lim_{t\to\infty} d_{\mathbb{X}\backslash\sim}([x(t)], [x]^\star_{+,+}(t)) = \lim_{t\to\infty} d_{\mathbb{X}\backslash\sim}(h(y(t)), h(y^\star_{+,+}(t))) = 0$*, which completes the proof.*

Theorem 16. *Consider the closed loop vector field* X^{cl} *in* (38)*, constructed assuming that the controllers in Assumption 12 are provided. Then, along solutions of*

$$\dot{x}(t) = X^{cl}(t, x(t)), \text{ with } x(0) \in \mathbb{X}, \tag{41}$$

it follows that, for some equilibrium equivalence class $[x]^\star_\star \in \{[x]^\star_{+,+}, [x]^\star_{-,+}, [x]^\star_{+,-}, [x]^\star_{-,-}\}$,

$$\lim_{t\to\infty} d_{\mathbb{X}\backslash\sim}([x(t)], [x]^\star_\star(t)) = 0, \tag{42}$$

where the equilibria equivalence classes are defined in (35) *and the distance* $d_{\mathbb{X}\backslash\sim}$ *is defined in* (14)*; i.e., it follows that the position tracking problem in Problem 1 is satisfied while the orientation tracking is not necessarily satisfied. Moreover, the equilibria equivalence classes* $[x]^\star_{-,+}$, $[x]^\star_{+,-}$ *and* $[x]^\star_{-,-}$ *are all unstable.*

Proof 17. *Proving the first part of the Theorem follows the same steps as in the proof of Theorem 14, which are therefore omitted. For the instability of* $[x]^\star_{-,+}$, $[x]^\star_{+,-}$ *and* $[x]^\star_{-,-}$*, it suffices to invoke instability of* $y^\star_{1-}$ *and* $y^\star_{2-}$ *and continuity of the map* h.

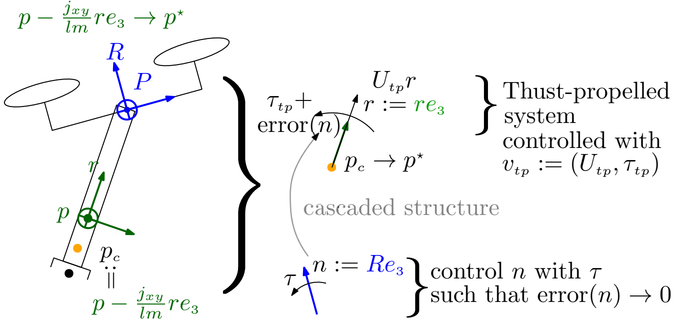

Figure 7: By means of appropriate state and input transformations, the UAV-slung-manipulator may be understood as two systems in cascade: one thrust-propelled system followed by one unit-vector double-integrator system.

6. UAV-slung-manipulator

We verify next that the UAV-slung-manipulator system behaves as a thrust-propelled system cascaded after a unit vector double integrator, as illustrated in Fig. 7. The three steps we follow next have been described in the Section 4.

6.1. State transformation

Recall the discussion from Section 4. Let us then introduce the set $\mathbb{Y}$ defined as (you may read the subindex tp as thrust-propelled)

$$\mathbb{Y}_{tp} := \left\{(p_c, v_c, r, \omega) \in (\mathbb{R}^3)^4 : r^T r = 1, r^T\omega = 0\right\}, \tag{43a}$$

$$\mathbb{Y} := \left\{(y_{tp}, (n, \varpi)) \in \mathbb{Y}_{tp} \times (\mathbb{R}^3)^2 : n^T n = 1, n^T \varpi = 0\right\}, \tag{43b}$$

with the inherited distances $d_{\mathbb{Y}_{tp}} := d_{\mathbb{R}^{12}}$ and $d_{\mathbb{Y}} := d_{\mathbb{R}^{18}}$ (the set $\mathbb{Y}_{tp}$ will be used for the part of the system that resembles a thrust-propelled system – see Fig. 7). For convenience, hereafter, we decompose elements in the sets above as

$$y_{tp} \in \mathbb{Y}_{tp} :\Leftrightarrow (p_c, v_c, r, \omega) \in \mathbb{Y}_{tp}, \tag{44a}$$

$$y \in \mathbb{Y} :\Leftrightarrow (y_{tp}, n, \varpi) \in \mathbb{Y}. \tag{44b}$$

Hereafter, we denote as well

$$v_{tp} \in \mathbb{R}^4 :\Leftrightarrow (U_{tp}, \tau_{tp}) \in \mathbb{R} \times \mathbb{R}^3, \tag{45a}$$

$$v \in \mathbb{R}^4 :\Leftrightarrow (U_{tp}, \tau) \in \mathbb{R} \times \mathbb{R}^3, \tag{45b}$$

where v_{tp} will be an auxiliary input (to the thrust propelled system), and v will be the actual input to the whole system.

Assumption 18. *At this point, we must make the assumption that either $j_{zz} = 0$ (i.e., that the manipulator is infinitesimally slender) or that $e_3^T\omega(0) = 0$ (i.e., that the manipulator is not initially spinning around itself). As part of future work, we wish to study how to overcome these assumptions; and, if the latter is not possible, to study how the tracking performance is affected when none of these assumptions is satisfied. Based on Proposition 1, it follows that if $e_3^T\omega(0) = 0$ then $e_3^T\omega(t) = 0$ for all $t \in \mathbb{R}$, i.e., that the manipulator remains without spinning around itself, and thus, hereafter, we restrict a state of the UAV-slung-manipulator system to be in the set $\{x \in \mathbb{X} : e_3^T\omega = 0\}$.*

Recall the definition of the state space $\mathbb{X}$ in (3), and the state decomposition in (4). Also, with Fig. 7 in mind, consider then the mapping

$$f : \mathbb{X}\backslash_{\sim} \ni [x] \mapsto f([x]) \in \mathbb{Y} \tag{46}$$

$$f([x]) := \begin{bmatrix} p - \frac{j_{xy}}{lm} r e_3 \\ v - \frac{j_{xy}}{lm} r \mathcal{S}(\omega) e_3 \\ r e_3 \\ \Pi(r e_3) r\omega \\ \hdashline R e_3 \\ \Pi(R e_3) R\Omega \end{bmatrix} \left(= \begin{bmatrix} p_c \\ v_c \\ r \\ \omega \\ \hdashline n \\ \varpi \end{bmatrix} = \begin{bmatrix} y_{tp} \\ \hdashline n \\ \varpi \end{bmatrix} = y \right),$$

and consider as well the mapping

$$h : \mathbb{Y} \ni y \mapsto h(y) \in \mathbb{X}\backslash_{\sim} \tag{47}$$

$$h(y) := \underbrace{\begin{bmatrix} p_c + \frac{j_{xy}}{lm} r \\ \tilde{r} \\ p_c + (\frac{j_{xy}}{lm} + l) r \\ \tilde{R} \\ \hdashline v_c + \frac{j_{xy}}{lm} \mathcal{S}(\omega) r \\ \tilde{r}^T\omega \\ v_c + (\frac{j_{xy}}{lm} + l)\mathcal{S}(\omega) r \\ \tilde{R}^T\varpi \end{bmatrix}}_{\substack{\text{where } \tilde{r}\in\mathbb{SO}(3) \text{ is s.t. } \tilde{r}e_3 = r \\ \text{where } \tilde{R}\in\mathbb{SO}(3) \text{ is s.t. } \tilde{R}e_3 = n}} \left(= \begin{bmatrix} p \\ r \\ P \\ R \\ \hdashline v \\ \omega \\ V \\ \Omega \end{bmatrix} = [x] \right),$$

where $[\cdot]$ above denotes the equivalence class as defined immediately after (13).

Proposition 19. *The map f in (46) is well defined, and*

$$f \circ h = id_{\mathbb{Y}} \text{ and } h \circ f = id_{\mathbb{X}\backslash_{\sim}}, \tag{48}$$

i.e., $h = f^{-1}$ and $f = h^{-1}$.

The proof follows the same steps as those in the proof of Proposition 10.

6.2. Input transformation

Let us construct the input transformation in two steps. For that purpose, consider the transformed dynamics with the original input (not the transformed input), which are given by

$$\dot{y} = Df([x])X(x,u) \Leftrightarrow \tag{49}$$

$$\begin{bmatrix} \dot{y}_{tp} \\ \hdashline \dot{n} \\ \dot{\varpi} \end{bmatrix} = \begin{bmatrix} \dot{p}_c \\ \dot{v}_c \\ \dot{r} \\ \dot{\omega} \\ \hdashline \dot{n} \\ \dot{\varpi} \end{bmatrix} = \begin{bmatrix} v - \frac{j_{xy}}{lm} r \mathcal{S}(\omega) e_3 \\ r e_3(\star_1) - g e_3 \\ \mathcal{S}(\Pi(r e_3) r\omega) r e_3 \\ \frac{l}{j_{xy}} \mathcal{S}(r e_3) T(x,u) \\ \hdashline \mathcal{S}(\Pi(R e_3) R\Omega) R e_3 \\ \Pi(R e_3) R(\star_2) \end{bmatrix},$$

$$(\star_1) = \frac{1}{m}(r e_3)^T T(x,u) + \frac{j_{xy}}{lm}\omega^T \Pi(e_3)\omega,$$

$$(\star_2) = J^{-1}(\tau - \mathcal{S}(\Omega) J\Omega) - e_3^T \mathcal{S}(\Omega) e_3.$$

Equation (49) sheds some light into how to design the controller. Suppose for now that we had control over the internal tensions – $T(x,u)$ (which we do, by intermediate of the input u; however we do not have control over all of the three components of $T(x,u)$). Then, one can choose the component of those tensions aligned with the manipulator axis of axial symmetry (i.e., $(re_3)^T T(x,u)$) in a way that behaves as a thrust in the differential equation $\dot{v}_c$ in (49);

one can also choose the components of those tensions orthogonal to the manipulator's axis of axial symmetry (i.e., $\Pi\left(re_3\right)T(x,u)$) in a way that behaves as a torque on the manipulator axis of symmetry – see the differential equation $\dot{\omega}$ in (49). With the above in mind, and $\dot{v}_c$ and $\dot{\omega}$ in (49) also in mind, we define

$$T^{cl}:\mathbb{Y}_{tp}\times\mathbb{R}^4\ni(y_{tp},v_{tp})\mapsto T^{cl}(y_{tp},v_{tp})\in\mathbb{R}^3 \tag{50}$$

$$T^{cl}(y_{tp},v_{tp}):=\frac{1}{m}\left(U_{tp}-\frac{j_{xy}}{lm}\omega^T\omega\right)r-\frac{j_{xy}}{l}\mathcal{S}\left(r\right)\tau_{tp}.$$

It then follows that

$$\dot{y}\quad=Df([x])X(x,u)|_{T(x,u)=T^{cl}(y_{tp},v_{tp})}|_{x\in h(y)}\Leftrightarrow$$

$$\begin{bmatrix}\dot{p}_c\\ \dot{v}_c\\ \dot{r}\\ \dot{\omega}\\ \dot{n}\\ \dot{\varpi}\end{bmatrix}=\begin{bmatrix}v_c\\ U_{tp}r-ge_3\\ \mathcal{S}\left(\omega\right)r\\ \mathcal{S}\left(r\right)\tau_{tp}\\ \star\\ \star\end{bmatrix}. \tag{51}$$

(The equation above is strictly speaking ill-defined, specifically the last element $\dot{\varpi}$ depends on the choice of representative $x\in h(y)\in\mathbb{X}\backslash_{\sim}$; the correct formulation is found later in (60)).

However, we do not have full control over the internal tensions, which is simple to verify by inspecting of T in (6a): the tensions are three dimensional ($T(x,u)\in\mathbb{R}^3$), and the only input that acts on the tensions is the one-dimensional thrust ($U\in\mathbb{R}$). Moreover, by inspection of T in (6a), notice the affine dependence on URe_3, which motivates us to introduce an extra dummy variable U_{3d} such that $URe_3=U_{3d}+(URe_3-U_{3d})$; with this in mind, notice that $T(x,u)$ in (6a) is equivalently written as (recall that in the UAV-slung-manipulator system $\tau_m=0_3$ and $e_3^T\omega=0$ – see Assumption 18)

$$T(x,u)=rA_T^{-1}r^T\left(U_{3d}+lM\omega^T\omega re_3+(URe_3-U_{3d})\right),$$

$$A_T\equiv\frac{m+M}{m}I_3+\frac{Ml^2}{j_{xy}}\Pi\left(e_3\right). \tag{52}$$

Loosely speaking, since we wish that $T(x,u)=T^{cl}(y_{tp},v_{tp})$, it naturally leads to the definition of

$$U_{3d}^{cl}:\mathbb{Y}_{tp}\times\mathbb{R}^4\ni(y_{tp},v_{tp})\mapsto U_{3d}^{cl}(y_{tp},v_{tp})\in\mathbb{R}^3 \tag{53}$$

$$U_{3d}^{cl}(y_{tp},v_{tp}):=(rA_Tr^TT^{cl}(y_{tp},v_{tp})-lM\omega^T\omega re_3)|_{x\in h(y)}$$

$$\overset{(50)}{=}lM\gamma\left(\left(\frac{m+M}{M}\frac{U_{tp}}{l\gamma}-\omega^T\omega\right)r-\mathcal{S}\left(r\right)\tau_{tp}\right)$$

and, as such, if we take (52) with $U_{3d}=U_{3d}^{cl}(y_{tp},v_{tp})$, it follows that the tensions $T(x,u)$ in (6a) are equivalently written as

$$T(x,u)=T^{cl}(y_{tp},v_{tp})+rA_T^{-1}r^T(URe_3-U_{3d}^{cl}(y_{tp},v_{tp})), \tag{54}$$

for any $x\in\mathbb{X}$ and any $v_{tp}\in\mathbb{R}^4$, and where $(y_{tp},\star)=f([x])$ (see (46)). After simple computations, it then follows that for any $v_{tp}=(U_{tp},\tau_{tp})\in\mathbb{R}^4$,

$$\dot{y}\quad=Df([x])X(x,u)|_{T(x,u)\text{as in (54)}}|_{x\in h(y)}\Leftrightarrow \tag{55}$$

$$\Leftrightarrow\begin{bmatrix}\dot{p}_c\\ \dot{v}_c\\ \dot{r}\\ \dot{\omega}\\ \dot{n}\\ \dot{\varpi}\end{bmatrix}=(51)+\begin{bmatrix}0_{3\times3}\\ \frac{1}{m+M}rr^T\\ 0_{3\times3}\\ \frac{1}{lM\gamma}\mathcal{S}\left(r\right)\\ 0_{3\times3}\\ 0_{3\times3}\end{bmatrix}(Un-U_{3d}^{cl}(y_{tp},v_{tp})).$$

A common and *natural* choice for the input U in (55) is one that minimizes the error $Un-U_{3d}^{cl}(y_{tp},u_{tp})$, i.e.,

$$\{n^TU_{3d}^{cl}(y_{tp},v_{tp})\}=\arg\min_{U\in\mathbb{R}}\|Un-U_{3d}^{cl}(y_{tp},v_{tp})\|.$$

This choice, despite *natural*, is not ideal, since, if this choice is made, it results in

$$\dot{v}_c=U_{tp}r-ge_3-\frac{1}{m+M}rr^T\Pi\left(n\right)U_{3d}^{cl}(y_{tp},v_{tp}),$$

which prevents us from using control laws in the literature which rely on the cascaded structure of the thrust-propelled system.

The other option (it comes at a cost we explain next) is one where U is chosen such that the acceleration $\dot{v}_c$ in (55) depends solely on the thrust U_{tp}, i.e., such that $r^T(Un-U_{3d}^{cl}(y_{tp},v_{tp}))$ vanishes. That leads to the definition of the control law

$$U^{cl}:\tilde{\mathbb{X}}\times\mathbb{R}\ni(x,U_{tp})\mapsto U^{cl}(x,U_{tp})\in\mathbb{R} \tag{56}$$

$$U^{cl}(x,U_{tp}):=\frac{r^TU_{3d}^{cl}(y_{tp},v_{tp})}{r^Tn}|_{y=f([x])\text{ and }v_{tp}=(U_{tp},\cdot)}$$

$$\overset{(53)}{=}\frac{(m+M)U_{tp}-lM\gamma\omega^T\omega}{(re_3)^T(Re_3)},$$

where

$$\tilde{\mathbb{X}}:=\{x\in\mathbb{X}:(re_3)^T(Re_3)\neq0\}. \tag{57}$$

The cost of this choice is now clear: the control law is not defined in the whole state space; in fact, it is not defined when the manipulator arm is orthogonal to the thrust axis of the UAV. Notice, however, that, since the UAV and manipulator have physical volume, the manipulator should therefore never be orthogonal to the thrust axis of the UAV, since in this case the two rigid bodies would collide.

Again, after simple computations, it follows that for any $v_{tp}=(U_{tp},\tau_{tp})\in\mathbb{R}^4$,

$$\dot{y}\quad=Df([x])X(x,u)|_{U=U^{cl}(x,U_{tp})}|_{x\in h(y)}\Leftrightarrow \tag{58}$$

$$\Leftrightarrow\begin{bmatrix}\dot{p}_c\\ \dot{v}_c\\ \dot{r}\\ \dot{\omega}\\ \dot{n}\\ \dot{\varpi}\end{bmatrix}=(51)+\frac{1}{lM\gamma}\frac{\Pi\left(r\right)}{r^Tn}\begin{bmatrix}0_{3\times3}\\ 0_{3\times3}\\ 0_{3\times3}\\ I_{3\times3}\\ 0_{3\times3}\\ 0_{3\times3}\end{bmatrix}\mathcal{S}\left(n\right)U_{3d}^{cl}(y_{tp},v_{tp}).$$

At this point, we can now introduce the input transformation. Given some $x\in\tilde{\mathbb{X}}$ and some $\tau_\psi\in\mathbb{R}$, consider then (see the input decomposition in (45))

$$\bar{u}_x^{cl}:\mathbb{U}\to\mathbb{U} \tag{59}$$

$$\bar{u}_x^{cl}(v):=\begin{bmatrix}U^{cl}(x,U_{tp})\\ J(\Pi\left(e_3\right)R\tau+\tau_\psi e_3+e_3^T\Omega\mathcal{S}\left(\Omega\right)e_3)-\mathcal{S}\left(\Omega\right)J\Omega\end{bmatrix}.$$

Given the input transformation $\bar{u}_x^{cl}$ in (59) and the state transformation f in (46) one can then compute the transformed dynamics, specifically

$$Y:\mathbb{Y}\times\mathbb{U}\ni(y,v)\mapsto Y(y,v)\in T_y\mathbb{Y} \tag{60}$$

$$
\dot{y} = Y(y, v) := Df([x])X(x, \bar{u}_x^{cl}(x, v, \cdot))|_{x \in h(y)} \Leftrightarrow
$$

$$
\begin{bmatrix} \dot{p}_c \\ \dot{v}_c \\ \dot{r} \\ \dot{\omega} \\ \dot{n} \\ \dot{\varpi} \end{bmatrix} = \begin{bmatrix} v_c \\ U_{tp} r - g e_3 \\ \mathcal{S}(\omega) r \\ \frac{1}{r^T n}\left(\frac{(m+M)}{lM\gamma} U_{tp} - \omega^T \omega\right) \mathcal{S}(r) n \\ \mathcal{S}(\varpi) n \\ \Pi(n) \tau \end{bmatrix}
$$

which, for any $\tau_{tp} \in \mathbb{R}^3$, is equivalently expressed as

$$
\begin{bmatrix} \dot{p}_c \\ \dot{v}_c \\ \dot{r} \\ \dot{\omega} \\ \dot{n} \\ \dot{\varpi} \end{bmatrix} = \begin{bmatrix} v_c \\ U_{tp} r - g e_3 \\ \mathcal{S}(\omega) r \\ \Pi(r) \tau_{tp} + \frac{\mathcal{S}(r)\mathcal{S}(n) U_{3d}^{cl}(y_{tp}, v_{tp})}{\gamma l M r^T n} \\ \mathcal{S}(\varpi) n \\ \Pi(n) \tau \end{bmatrix}. \tag{61}
$$

The cascaded structure of the vector field Y is now clear, since Y can be equivalently written as (below, and for brevity, $0 \equiv 0_{3\times 3}$ and $I \equiv I_3$)

$$
\begin{bmatrix} \dot{p}_c \\ \dot{v}_c \\ \dot{r} \\ \dot{\omega} \\ \dot{n} \\ \dot{\varpi} \end{bmatrix} = \begin{bmatrix} 0 & I & 0 & 0 & 0 & 0 \\ 0 & 0 & U_{tp} I & 0 & 0 & 0 \\ 0 & 0 & 0 & -\mathcal{S}(r) & 0 & 0 \\ 0 & 0 & 0 & 0 & (\star)\mathcal{S}(r) & 0 \\ 0 & 0 & 0 & 0 & 0 & -\mathcal{S}(n) \\ 0 & 0 & 0 & 0 & 0 & 0 \end{bmatrix} \begin{bmatrix} p_c \\ v_c \\ r \\ \omega \\ n \\ \varpi \end{bmatrix} + \begin{bmatrix} 0_3 \\ -g e_3 \\ 0_3 \\ 0_3 \\ 0_3 \\ \Pi(n) \tau \end{bmatrix},
$$

$(\star) = \frac{1}{r^T n}\left(\frac{(m+M)}{\gamma} U_{tp} - \omega^T \omega\right)$.

Recall then Problem 2. For reasons that will be clear next, we require the desired position trajectory $p^\star$ to satisfy some constraints, specifically

$$
p^\star \in \mathcal{C}^6, \sup_{t \in \mathbb{R}} p^{\star(i)}(t) < \infty \text{ for } i \in \{2, 3, 4, 5, 6\}, \tag{62a}
$$

$$
\inf_{t \in \mathbb{R}} \|p^{\star(2)}(t) + g e_3\| > 0, \tag{62b}
$$

$$
\inf_{t \in \mathbb{R}} \left\{ \begin{matrix} \|\Pi(r^\star(t)) \ddot{r}^\star(t)\|^2 + \\ \left(\|\mathcal{S}(r^\star(t)) \dot{r}^\star(t)\|^2 \pm \frac{1}{\gamma} \frac{(m+M)}{M} \frac{\|\ddot{p}^\star(t) + g e_3\|}{l}\right)^2 \end{matrix} \right\} > 0, \tag{62c}
$$

where $r^\star(t) \equiv \frac{p^{\star(2)}(t) + g e_3}{\|p^{\star(2)}(t) + g e_3\|}$. We say that a trajectory $p^\star$ is *feasible* if it satisfies the constraints in (62). Loosely speaking, feasible trajectories are those whose high-order derivatives (in particular, $p^{\star(2)}, p^{\star(3)}, p^{\star(4)}$) are *small* in magnitude (where *small* is quantified in (62)). In particular, if we take those high order derivatives to be zero (constant speed trajectory), the constraints (62b) and (62c) read as $\sup_{t \in \mathbb{R}} \|g e_3\| > 0$ and as $\sup_{t \in \mathbb{R}} \left(\pm \frac{1}{\gamma} \frac{(m+M)}{M} \frac{\|g e_3\|}{l}\right)^2 > 0$, which are indeed satisfied.

6.3. Differential flatness

It follows from the cascaded structure of the vector field Y in (60) that it is differentially flat with respect to the position p_c; equivalently, it follows that the vector field X in (15) (if we ignore rotations of the rigid bodies around their third axes) is differentially flat with respect to the position $p - \frac{j_{xy}}{lm} r e_3$ (this justifies the claim in Remark 7). Indeed, if we require $t \mapsto p_c(t) := p^\star(t)$, then we find *four* equilibria state trajectories and *two* equilibria input trajectories, namely (below $y^\star_{\pm,\mp}$ stands for four solutions, namely $y^\star_{+,+}$, $y^\star_{-,+}$, $y^\star_{+,-}$ and $y^\star_{-,-}$)

$$
y^\star_{\pm,\mp} : \mathbb{R} \ni t \mapsto y^\star_{\pm,\mp}(t) \in \mathbb{Y} \tag{63}
$$

$$
y^\star_{\pm,\mp}(t) := \begin{bmatrix} y^\star_{tp,\pm} \\ \hdashline n^\star_{\pm,\mp}(t) \\ \varpi^\star(t) \end{bmatrix} := \begin{bmatrix} p^\star_c(t) \\ v^\star_c(t) \\ r^\star_\pm(t) \\ \omega^\star(t) \\ \hdashline n^\star_{\pm,\mp}(t) \\ \varpi^\star(t) \end{bmatrix} := \begin{bmatrix} p^{\star(0)}(t) \\ p^{\star(1)}(t) \\ \pm \frac{p^{\star(2)}(t) + g e_3}{\|p^{\star(2)}(t) + g e_3\|} \\ \mathcal{S}\left(r^\star_\pm(t)\right) r^{\star(1)}_\pm(t) \\ \hdashline \mp \frac{U^{cl}_{3d}(y^\star_{tp,\pm}(t), u^\star_{tp,\pm}(t))}{\|U^{cl}_{3d}(y^\star_{tp,\pm}(t), u^\star_{tp,\pm}(t))\|} \\ \mathcal{S}\left(n^\star_{\pm,\mp}(t)\right) n^{\star(1)}_{\pm,\mp}(t) \end{bmatrix},
$$

$$
u^\star_{tp,\pm}(t) := \begin{bmatrix} U^\star_{tp}(t) \\ \tau^\star_{tp}(t) \end{bmatrix} := \begin{bmatrix} \pm\|p^{\star(2)}_c(t) + g e_3\| \\ \omega^{\star(1)}(t) \end{bmatrix},
$$

and (below we use the definition of $\varpi^\star$ presented above)

$$
v^\star_\pm : \mathbb{R} \to \mathbb{R}^4, v^\star_\pm(t) := \begin{bmatrix} \pm\|p^{\star(2)}_c(t) + g e_3\| \\ \varpi^{\star(1)}(t) \end{bmatrix}. \tag{64}
$$

(Notice that, despite the presence of $r^\star_\pm$ and $n^\star_{\pm,\mp}$ in the definition of $\omega^\star$ and $\varpi^\star$ (respectively), these are independent of the choice of sign).

It should now be clear from (63), specifically from the definition of $r^\star_\pm$ and $n^\star_{\pm,\mp}$, why the desired position trajectory $p^\star$ was required to satisfy the constraints (62b) and (62c) (in particular, (62c) is equivalently expressed as $\sup_{t\in\mathbb{R}} \|U^{cl}_{3d}(y^\star_{tp,\pm}(t), u^\star_{tp,\pm}(t))\| > 0$). Intuitively, (62b) guarantees that the desired attitude of the manipulator third axis is well defined; and (62c) guarantees that the desired attitude of the UAV third axis is well defined.

The equilibria $\{y^\star_{+,+}, y^\star_{-,+}, y^\star_{+,-}, y^\star_{-,-}\}$ just defined allows us to compute four equilibria in the original system apart from rotations around the rigid bodies' third axes; i.e., it allows us to compute four equilibria equivalence classes (which we denote by $\{[x]^\star_{+,+}, [x]^\star_{-,+}, [x]^\star_{+,-}, [x]^\star_{-,-}\}$), with the help of the map h in (47), namely

$$
[x]^\star_{\pm,\mp} : \mathbb{R} \ni t \mapsto [x]^\star_{\pm,\mp}(t) := h(y^\star_{\pm,\mp}(t)) \in \mathbb{X}\backslash_\sim. \tag{65}
$$

See Remark 20 in [39] for why one should not specify a desired trajectory for the UAV's (or the manipulator's) position: if that is specified, then there exist infinite equilibria equivalence class trajectories (rather than just four), where the manipulator behaves as a pendulum whose base is the UAV position (or the manipulator's) with a pendulum length $l' = \frac{j_{xy}}{lm} + l$ (or $l' = \frac{j_{xy}}{lm}$).

Assumption 20. *With the equilibria $y^\star_{\pm,\mp}$ in (63) in mind, we assume there exists a controller*

$$
v^{cl} : \mathbb{R} \times \mathbb{Y} \to \mathbb{R}^4,
$$

and non-empty $\mathbb{Y}_0 \subset \mathbb{Y}$, such that along solutions of

$$
\dot{y}(t) = Y(y(t), v^{cl}(t, y(t))), y(0) \in \mathbb{Y}_0,
$$

it holds that (i) $t \mapsto y(t)$ does not approach the boundary of $\{y \in \mathbb{Y} : r^T n > 0\}$; that (ii) $y^\star_{+,+}$ is stable; and that (iii)

$$
\lim_{t\to\infty} (y(t) - y^\star_{+,+}(t)) = 0_{18}.
$$

Finally, we assume that the equilibria trajectories $y^\star_{-,+}$, $y^\star_{+,-}$ and $y^\star_{-,-}$ are unstable.

Note that the vector field Y in (61) is that of a VTOL vehicle cascaded after a second order system in the unit sphere. For this vector field, we are able to leverage controllers for VTOL vehicles from the literature [41, 45, 51, 52], which must be complemented with two backstepping steps (related to the second order system). As such, Assumption 20 is indeed satisfied if the desired position trajectory satisfies the constraints in (62), i.e., a controller can be found that satisfies the conditions in the assumption.

Let us then present the result that guarantees that Problem 2 is accomplished. For that purpose, let Assumption 20 be satisfied, and construct the control law u^{cl} as a composition of the input transformation $\bar{u}^{cl}_x$ in (59) with the control law presented in Assumption 20, i.e.,

$$u^{cl} : \mathbb{R} \times \mathbb{X} \ni (t,x) \mapsto u^{cl}(t,x) \in \mathbb{R}^4 \quad (66)$$
$$u^{cl}(t,x) = \bar{u}^{cl}_x(v^{cl}(t,y))|_{y=f([x])},$$

which leads to the closed loop vector field

$$\mathbb{R} \times \mathbb{X} \ni (t,x) \mapsto X^{cl}(t,x) := X(x, u^{cl}(t,x)) \in T_x\mathbb{X}. \quad (67)$$

Theorem 21. *Consider the closed loop vector field X^{cl} in (67), constructed under the assumption that the controllers in Assumption 20 are provided. Then, along solutions of*

$$\dot{x}(t) = X^{cl}(t,x(t)), \text{ with } [x(0)] \in h(\mathbb{Y}_0) \quad (68)$$

where $h(\mathbb{Y}_0) := \{h(y) \in \mathbb{X}\backslash_\sim : y \in \mathbb{Y}_0\}$, it follows that

$$\lim_{t\to\infty} d_{\mathbb{X}\backslash_\sim}([x(t)], [x]^\star_{+,+}(t)) = 0, \quad (69)$$

with the equilibrium equivalence class $[x]^\star_{+,+}$ defined in (65) and the distance $d_{\mathbb{X}\backslash_\sim}$ defined in (14). That is, it follows that Problem 1 is satisfied. Moreover, the equilibria equivalence classes $[x]^\star_{-,+}$, $[x]^\star_{+,-}$ and $[x]^\star_{-,-}$ are all unstable.

Proof 22. *Since $[x(0)] \in h(\mathbb{Y}_0)$ it follows that $y(0) := f([x(0)]) \in \mathbb{Y}_0$; moreover, if we apply the control law (66), then the conclusions in Assumption 20 hold. Because $t \mapsto y(t) = f([x(t)]) \Leftrightarrow t \mapsto [x(t)] = h(y(t))$, it follows that the same logic chain as in the proof of Theorem 14 follows, which completes the proof.*

7. Simulations

Let us provide simulations that illustrate stability, convergence and robustness results. The physical constants were taken as $m = 0.3$kg, $M = 1.4$kg, $j = 0.007 \oplus 0.007 \oplus 0.001$kg m^2 and $J = 0.01 \oplus 0.01 \oplus 0.2$kg m^2; and with $l = 0.5$m for the UAV-manipulator system and with $l = 0.9$m for the UAV-slung-manipulator system. The specific control laws v^{cl}, as presented in Assumptions 12 and 20, are detailed in the mathematica files [39] (including the choice of gains; the chosen controller follows the structure described in [45]). We provide two simulations, in Figs. 8 and 9, one for each system; these are obtained as the solution to $\dot{x}(t) = X^{cl}(t,x(t))$ with initial condition $x(0) = (0_3, I_3, le_3, I_3, 0_3, 0_3, 0_3, 0_3) \in \mathbb{X}$ ($x(0)$ in SI units) and where some of the controller parameters have been disturbed (namely, the manipulator's mass and moments of inertia: $m_{\text{controller}} = 0.9m_{\text{model}}$ and $j_{\text{controller}} = 0.8j_{\text{model}}$). For the desired position trajectory, we have chosen (Problems 1 and 2)

$$t \mapsto p^\star(t) := \left(2\cos\left(\tfrac{2\pi}{8}t\right), 2\sin\left(\tfrac{2\pi}{8}t\right), 0.2 + 0.2\cos\left(\tfrac{2\pi}{4}t\right)\right),$$

corresponding to a circle of $2m$ radius in the horizontal plane and with a period of $12s$, superimposed with an oscillatory motion in the vertical direction with an amplitude of $0.2m$ and with a period of $6s$; and for the desired

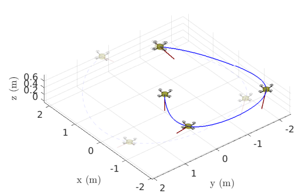

(a) Trajectory (desired in transparent), from 0 to 7 sec.

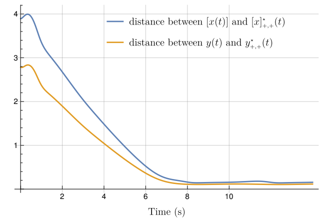

(b) Distance between real and equilibrium trajectories.

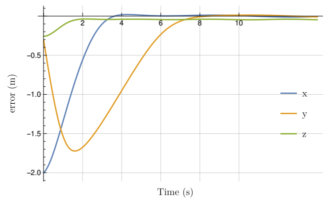

(c) Error position for center-of-mass $\frac{mp+MP}{m+M}$.

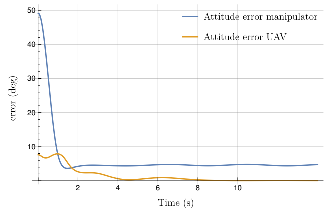

(d) Manipulator and UAV attitude errors

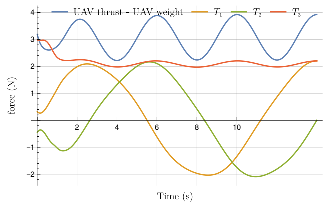

(e) UAV thrust input and internal forces.

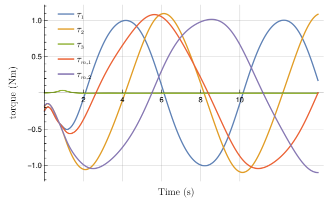

(f) UAV torque input and manipulator torque input.

Figure 8: Simulation for UAV-manipulator system with disturbed parameters (manipulator's mass and moments of inertia): $m_{\text{controller}} = 0.9m_{\text{model}}$ and $j_{\text{controller}} = 0.8j_{\text{model}}$.

orientation trajectory, we have chosen (Problem 1)

$$t \mapsto r^\star(t) := \tfrac{2}{\sqrt{7}}\left(-\sin\left(\tfrac{2\pi}{8}t\right), \cos\left(\tfrac{2\pi}{8}t\right), \cos\left(\tfrac{\pi}{6}\right)\right) \in \mathbb{S}^2,$$

corresponding to an orientation trajectory where the desired manipulator is tilted 30° away from the vertical direction, and where the manipulator is tangent (when seen from the top) to the horizontal motion of $p^\star$.

Fig. 8 is related to the UAV-manipulator system, and Fig. 9 is related to the UAV-slung-manipulator system.

In Figs. 8a and 9a, one can visualize the real system pose (pose of both rigid bodies – the UAV's and the manipulator's) in opaque, and the equilibrium system pose in transparent. In Figs. 8b and 9b, one can visualize the distance between the equivalence-class trajectory $t \mapsto [x(t)]$ and the stable equilibrium equivalence-class trajectory $t \mapsto [x]^\star_{+,+}(t)$ as defined in (35) and (65), and by means of the distance $d_{\mathbb{X}\backslash_\sim}$ defined in (14); as well as the distance between the transformed trajectory $t \mapsto y(t) := f(x(t))$ and the stable equilibrium transformed trajectory $t \mapsto y^\star_{+,+}(t)$ as defined in (35) and (63) (and by means of the distance $d_{\mathbb{Y}} := d_{\mathbb{R}^{18}}$). Notice that these distances may increase, during some time intervals, but they converge to zero asymptotically in the absence of parameters' mismatch.

In Figs. 8c and 9c, the position error is shown for the positions of the thrust propelled systems, i.e., the center-of-mass position error $(t \mapsto \frac{mp(t)+MP(t)}{m+M} - p^\star_{cm}(t))$ for the UAV-manipulator system, and the position error $t \mapsto p(t) - \frac{j_{xy}}{lm} r(t)e_3 - p^\star(t)$ for the UAV-slung-manipulator system. In Figs. 8d and 9d, the manipulator attitude error $(t \mapsto \arccos((r(t)e_3)^T r^\star_+(t)))$, and the UAV attitude error $(t \mapsto \arccos((R(t)e_3)^T n^\star(t)))$ are shown ($n^\star \equiv n^\star_+$ in Fig. 8d, and $n^\star \equiv n^\star_{+,+}$ in Fig. 9d). The position errors settle around 5 cm, while the orientation errors settle around 5 degrees; we note, however, that they converge to zero in the absence of parameters' mismatch. As such, these simulations provide some insight into the robustness of the controllers with respect to model parameters mismatch. Moreover, the errors described above can be made smaller than some prescribed upper bound either by choosing bigger gains, or by including integral action terms.

In Figs. 8e–8f and Figs. 9e–9f, the input as obtained from the proposed control law $t \mapsto u^{cl}(t, x(t))$ is shown, with u^{cl} as defined in (37) and in (66). Finally, in Figs. 8e and 9e, the internal forces $t \mapsto T(x(t), u^{cl}(t, x(t)))$ (with T as defined in (6a)) are shown. We emphasize only that the tension along the manipulator third axis is, in general, bigger than the others, since, loosely speaking, this is the component that needs to *cancel* the manipulator's weight.

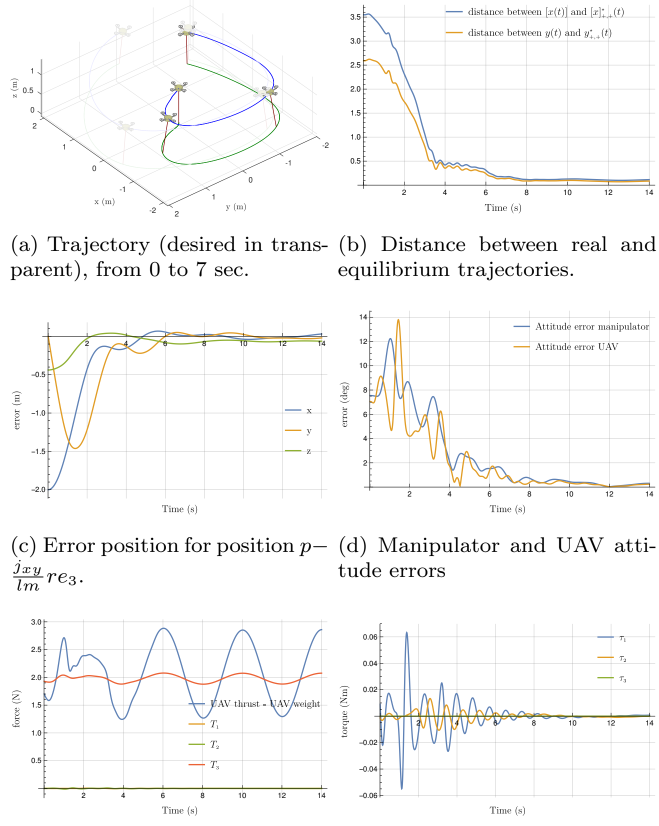

(a) Trajectory (desired in transparent), from 0 to 7 sec.

(b) Distance between real and equilibrium trajectories.

(c) Error position for position $p - \frac{j_{xy}}{lm} re_3$.

(d) Manipulator and UAV attitude errors

(e) UAV thrust input and internal forces.

(f) UAV torque input.

Figure 9: Simulation for UAV-slung-manipulator system with disturbed parameters (manipulator's mass and moments of inertia): $m_{\text{controller}} = 0.9 m_{\text{model}}$ and $j_{\text{controller}} = 0.8 j_{\text{model}}$.

8. Conclusions

This manuscript focuses on pose tracking problems for a system composed of two connected rigid bodies, namely an aerial vehicle – with hovering capabilities – and a rod-like rigid body. When a torque input at the joint connecting the two rigid bodies is available, a semi-pose tracking problem is formulated, requiring the rod object to track a desired pose trajectory. When no such torque input is available, a position tracking problem is formulated, requiring a specific point along the axis of axial symmetry of the rod object to track a desired position trajectory. Our approach for solving both these problems lied in finding a state and an input transformations, such that the vector field in the new coordinates is of a known form for which controllers are found in the literature, and which we leveraged in this manuscript. In this paper, we assumed the joint connecting the two rigid-bodies is an ideal spherical joint: this assumption was made so as to simplify the analysis, but, in the future, we would like to consider *(i)* rotational constraints, *(ii)* how to design controllers that guarantee that those constraints are not violated, and *(iii)* studying the actual mechanical implementation of such an actuated joint. Finally, under the presence of model mismatches, we verified that there exists a non-zero steady state error, which may be removed with the addition of integral action terms. The effect and sensitivity of the proposed approach to measurement noise, filtering and delays is also a topic of future work.

[1] AEROWORKS aim. http://www.aeroworks2020.eu/.

[2] A. Wallar, E. Plaku, and D. A. Sofge. Reactive motion planning for unmanned aerial surveillance of risk-sensitive areas. *IEEE TASE*, 12(3):969–980, July 2015.

[3] A. Suarez, G. Heredia, and A. Ollero. Lightweight compliant arm with compliant finger for aerial manipulation and inspection. In *IEEE/RSJ IROS*, pages 4449–4454, Oct 2016.

[4] Markus Bernard, Konstantin Kondak, Ivan Maza, and Anibal Ollero. Autonomous transportation and deployment with aerial robots for search and rescue missions. *Journal of Field Robotics*, 28(6):914–931, 2011.

[5] I. Palunko, P. Cruz, and R. Fierro. Agile load transportation: Safe and efficient load manipulation with aerial robots. *IEEE Robotics Automation Magazine*, 19(3):69–79, Sept 2012.

[6] Konstantin Kondak, Markus Bernard, Fernando Caballero, Ivan Maza, and Anibal Ollero. Cooperative autonomous helicopters for load transportation and environment perception. *Advances in Robotics Research*, pages 299–310, 2009.

[7] M. Bisgaard, A. la Cour-Harbo, and J. D. Bendtsen. Adaptive control system for autonomous helicopter slung load operations. *Control Engineering Practice*, 18(7):800 – 811, 2010. SI on Aerial Robotics.

[8] M. Gassner, T. Cieslewski, and D. Scaramuzza. Dynamic collaboration without communication: Vision-based cable-suspended load transport with two quadrotors. In *IEEE ICRA*, pages 5196–5202, May 2017.

[9] I. Palunko, A. Faust, P. Cruz, L. Tapia, and R. Fierro. A reinforcement learning approach towards autonomous suspended load manipulation using aerial robots. In *IEEE ICRA*, pages 4896–4901, May 2013.

[10] P. Cruz and R. Fierro. Autonomous lift of a cable-suspended load by an unmanned aerial robot. In *IEEE CCA*, pages 802–

807, Oct 2014.

[11] P. J. Cruz, M. Oishi, and R. Fierro. Lift of a cable-suspended load by a quadrotor: A hybrid system approach. In *ACC*, pages 1887–1892, July 2015.

[12] F. A. Goodarzi and T. Lee. Dynamics and control of quadrotor UAVs transporting a rigid body connected via flexible cables. In *ACC*, pages 4677–4682, July 2015.

[13] T. Lee, K. Sreenath, and V. Kumar. Geometric control of cooperating multiple quadrotor UAVs with a suspended payload. In *52nd IEEE CDC*, pages 5510–5515, Dec 2013.

[14] T. Lee. Collision avoidance for quadrotor UAVs transporting a payload via Voronoi tessellation. In *ACC*, pages 1842–1848, July 2015.

[15] I. H. B. Pizetta, A. S. Brandão, and M. Sarcinelli-Filho. Modelling and control of a PVTOL quadrotor carrying a suspended load. In *2015 ICUAS*, pages 444–450, June 2015.

[16] Nathan Michael, Jonathan Fink, and Vijay Kumar. Cooperative manipulation and transportation with aerial robots. *Autonomous Robots*, 30(1):73–86, 2011.

[17] Guilherme V Raffo and Marcelino M de Almeida. Nonlinear robust control of a quadrotor UAV for load transportation with swing improvement. In *ACC*, pages 3156–3162. IEEE, 2016.

[18] P. Foehn, D. Falanga, N. Kuppuswamy, R. Tedrake, and D. Scaramuzza. Fast trajectory optimization for agile quadrotor maneuvers with a cable-suspended payload. In *Robotics: Science and Systems*, 2017.

[19] M. Tognon, C. Gabellieri, L. Pallottino, and A. Franchi. Aerial co-manipulation with cables: The role of internal force for equilibria, stability, and passivity. *IEEE Robotics and Automation Letters*, 3(3):2577–2583, July 2018.

[20] Khelifa Baizid, G Giglio, Francesco Pierri, Miguel Angel Trujillo, Gianluca Antonelli, Fabrizio Caccavale, Antidio Viguria, Stefano Chiaverini, and Aníbal Ollero. Behavioral control of unmanned aerial vehicle manipulator systems. *Autonomous Robots*, 41(5):1203–1220, 2017.

[21] S. Kim, S. Choi, and H. J. Kim. Aerial manipulation using a quadrotor with a two DOF robotic arm. In *IEEE/RSJ IROS*, pages 4990–4995, Nov 2013.

[22] H. Lee, H. Kim, and H. J. Kim. Planning and control for collision-free cooperative aerial transportation. *IEEE TASE*, PP(99):1–13, 2017.

[23] H. Kim, H. Lee, S. Choi, Y. k. Noh, and H. J. Kim. Motion planning with movement primitives for cooperative aerial transportation in obstacle environment. In *IEEE ICRA*, pages 2328–2334, May 2017.

[24] M. Tognon, B. Yüksel, G. Buondonno, and A. Franchi. Dynamic decentralized control for protocentric aerial manipulators. In *IEEE ICRA*, pages 6375–6380, May 2017.

[25] F. Ruggiero et al. A multilayer control for multirotor UAVs equipped with a servo robot arm. In *ICRA*, pages 4014–4020. IEEE, 2015.

[26] A. Jimenez-Cano, J. Martin, G. Heredia, A. Ollero, and R. Cano. Control of an aerial robot with multi-link arm for assembly tasks. In *ICRA*, pages 4916–4921. IEEE, 2013.

[27] C. Korpela, M. Orsag, M. Pekala, and P. Oh. Dynamic stability of a mobile manipulating unmanned aerial vehicle. In *ICRA*, pages 4922–4927, 2013.

[28] S. J. Lee and H. J. Kim. Autonomous swing-angle estimation for stable slung-load flight of multi-rotor UAVs. In *IEEE ICRA*, pages 4576–4581, May 2017.

[29] J. Thomas, G. Loianno, K. Sreenath, and V. Kumar. Toward image based visual servoing for aerial grasping and perching. In *IEEE ICRA*, pages 2113–2118, May 2014.

[30] R. Mebarki, V. Lippiello, and B. Siciliano. Toward image-based visual servoing for cooperative aerial manipulation. In *IEEE ICRA*, pages 6074–6080, May 2015.

[31] K. Sreenath, T. Lee, and V. Kumar. Geometric control and differential flatness of a quadrotor UAV with a cable-suspended load. In *52nd IEEE CDC*, pages 2269–2274, Dec 2013.

[32] K. Sreenath, N. Michael, and V. Kumar. Trajectory generation and control of a quadrotor with a cable-suspended load - a differentially-flat hybrid system. In *IEEE ICRA*, pages 4888–4895. IEEE, 2013.

[33] I. Palunko, R. Fierro, and P. Cruz. Trajectory generation for swing-free maneuvers of a quadrotor with suspended payload: A dynamic programming approach. In *IEEE ICRA*, pages 2691–2697, May 2012.

[34] M. Tognon and A. Franchi. Dynamics, control, and estimation for aerial robots tethered by cables or bars. *IEEE T-RO*, 33(4):834–845, Aug 2017.

[35] S. Tang and V. Kumar. Mixed integer quadratic program trajectory generation for a quadrotor with a cable-suspended payload. In *IEEE ICRA*, pages 2216–2222, May 2015.

[36] A. Tagliabue, M. Kamel, S. Verling, R. Siegwart, and J. Nieto. Collaborative transportation using mavs via passive force control. In *IEEE International Conference on Robotics and Automation*, pages 5766–5773, May 2017.

[37] Patricio J. Cruz and Rafael Fierro. Cable-suspended load lifting by a quadrotor UAV: hybrid model, trajectory generation, and control. *Autonomous Robots*, 41(8):1629–1643, Dec 2017.

[38] P. O. Pereira, R. Zanella, and D. V. Dimarogonas. Decoupled design of controllers for aerial manipulation with quadrotors. In *IEEE/RSJ IROS*, pages 4849–4855, Oct 2016.

[39] P. Pereira and Dimos V. Dimarogonas. Mathematica files used in obtaining the manuscript's results with a companion extended paper version. In *https://github.com/KTH-SML/aerial-generalized-slung-load-transportation.git*.

[40] Hanlei Wang and Yongchun Xie. Adaptive inverse dynamics control of robots with uncertain kinematics and dynamics. *Automatica*, 45(9):2114 – 2119, 2009.

[41] Minh-Duc Hua, Tarek Hamel, Pascal Morin, and Claude Samson. Introduction to feedback control of underactuated VTOL vehicles: A review of basic control design ideas and principles. *IEEE Control Systems*, 33(1):61–75, 2013.

[42] Abdelkader Abdessameud and Abdelhamid Tayebi. Global trajectory tracking control of VTOL-UAVs without linear velocity measurements. *Automatica*, 46(6):1053 – 1059, 2010.

[43] Minh-Duc Hua, Tarek Hamel, Pascal Morin, and Claude Samson. Control of VTOL vehicles with thrust-tilting augmentation. *Automatica*, 52:1 – 7, 2015.

[44] Pedro Casau, Ricardo G. Sanfelice, Rita Cunha, David Cabecinhas, and Carlos Silvestre. Robust global trajectory tracking for a class of underactuated vehicles. *Automatica*, 58:90 – 98, 2015.

[45] P. O. Pereira and D. V. Dimarogonas. Lyapunov-based generic controller design for thrust-propelled underactuated systems. In *ECC*, pages 594–599, June 2016.

[46] Haichao Gui and George Vukovich. Finite-time output-feedback position and attitude tracking of a rigid body. *Automatica*, 74:270 – 278, 2016.

[47] C. G. Mayhew, R. G. Sanfelice, and A. R. Teel. Quaternion-based hybrid control for robust global attitude tracking. *IEEE TAC*, 56(11):2555–2566, Nov 2011.

[48] Christopher G. Mayhew and Andrew R. Teel. Global stabilization of spherical orientation by synergistic hybrid feedback with application to reduced-attitude tracking for rigid bodies. *Automatica*, 49(7):1945 – 1957, 2013.

[49] P. O. Pereira, M. Herzog, and D. V. Dimarogonas. Slung load transportation with a single aerial vehicle and disturbance removal. In *24th MED*, pages 671–676, June 2016.

[50] Avian-inspired grasping for quadrotor micro UAVs.

[51] R. Naldi, M. Furci, R. G. Sanfelice, and L. Marconi. Robust global trajectory tracking for underactuated VTOL aerial vehicles using inner-outer loop control paradigms. *IEEE TAC*, 62(1):97–112, Jan 2017.

[52] M. D. Hua, T. Hamel, P. Morin, and C. Samson. A control approach for thrust-propelled underactuated vehicles and its application to VTOL drones. *IEEE TAC*, 54(8):1837–1853, Aug 2009.